ergy dispersion of the primary electrons. If the spread in primary energy is taken into account the inherent dispersion can be found for the various shower quantities. The results are listed in Table VIII(a). It is interesting to estimate the statistical accuracy within which the energy of one shower may be evaluated by observing such features as L_T, N_Σ, or $N_{\max}$. In Sec. 6 the average values of these quantities were found to have the behavior $n=CE_0^x$ hence $dE_0/E_0=x^{-1}\ dn/n$. The expected standard errors, dE_0/E_0, are listed in Table VII(b) for energies inferred from L_T, N_Σ, and $N_{\max}$. As might be expected, the use of N_Σ has some advantage in statistical precision over $N_{\max}$ and has the advantage over use of L_T, that N_Σ can be observed even at rather high energies with a chamber of modest dimensions.

ACKNOWLEDGMENTS

It is a pleasure to thank Professor Kenneth Greisen for many discussions and suggestions. I would also like to thank Professor R. R. Wilson for the use of his shower "histories" and Dr. E. Malamud and Dr. R. Schectman for their assistance in making these measurements.

PHYSICAL REVIEW VOLUME 136, NUMBER 2B 26 OCTOBER 1964

Parity and Sign of the $\Sigma^+ \to n+\pi^+$ Decay Amplitude and a Model for π^+ Emission in Hypernuclear Decays*

FRANK VON HIPPEL†

The Enrico Fermi Institute for Nuclear Studies, The University of Chicago, Chicago, Illinois

(Received 8 June 1964)

It is found that the π^+/π^- emission ratio of 0.029 ± 0.01 in ${}_\Lambda He^4$ can be understood as due to the combined mechanisms: decay of a virtual Σ^+ hypernuclear state and the charge exchange of a π^0 from neutral Λ decay. Improvements upon simple perturbation-calculational techniques give $\pi^+/\pi^-\approx0.015$ in near agreement with experiment, however, only if the decay $\Sigma^+ \to n+\pi^+$ is assumed to go to a final relative S state of the π^+ and neutron. Best agreement with experiment, for a D/F ratio of about 3 in the unitary symmetric strong pseudoscalar couplings, is obtained if the relative phases of the weak-decay amplitudes are determined according to unitary symmetry arguments. The observed low energy of the emitted π^+ mesons relative to the π^- mesons and the relative π^+ decay rates of different hypernuclei are qualitatively understood as primarily due to Pauli suppression effects in the final state. Reasons are given which suggest that the mesonic corrections to impulse-approximation calculations of the π^- and π^0 emission rates for the light hypernuclei will be small.

I. INTRODUCTION

WE consider here the simplest mechanisms which might account for the observed decay[1–7]

$$ {}_\Lambda He^4 \to (\text{nucleons})+\pi^+ \qquad (1.1)$$

and calculate the branching ratio of this mode (experimentally estimated[6] at about 0.029 ± 0.01) relative to the mode

$$ {}_\Lambda He^4 \to (\text{nucleons})+\pi^- \qquad (1.2)$$

for various assumptions concerning the strong and weak baryon-pion couplings. Our major result is that the observed rate for the decay (1.1) can be explained as due to constructive interference between the two processes represented in Fig. 1 which give $\pi^+/\pi^-\approx0.015$. The constructive interference is compatible with the relative phases of the nonleptonic decay interactions obtained by Lee[8] in fitting the experimental data to a

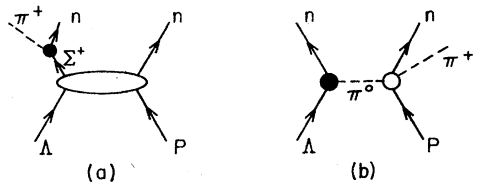

FIG. 1. Contributions found most important: (a) S-wave decay of a virtual Σ^+ state; (b) charge exchange on a proton of a π^0 from Λ decay.

* This work is supported by the U. S. Atomic Energy Commission

† Present address: Laboratory for Nuclear Science, Cornell University, Ithaca, New York.

[1] Y. W. Kang, N. Kwak, J. Schneps, and P. A. Smith, Nuovo Cimento **22**, 1297 (1961).

[2] A. Z. M. Ismail, I. R. Kenyon, A. W. Key, S. Lokanathan, and Y. Prakash, Phys. Letters **1**, 199 (1962).

[3] S. N. Ganguli, N. K. Rao, and M. S. Swami, Nuovo Cimento **28**, 1258 (1963).

[4] P. Allen, Sr., M. Heeran, and A. Montwill, Phys. Letters **3**, 274 (1963).

[5] P. H. Steinberg and R. J. Prem, Phys. Rev. Letters **11**, 429 (1963).

[6] M. J. Beniston, R. Levi-Setti, W. Püschel, and M. Raymund, Phys. Rev. **134**, B641 (1964).

[7] M. M. Block, R. Gessaroli, S. Ratti, L. Grimellini, T. Kikuchi, L. Lendinara, L. Monari, and E. Harth, Nuovo Cimento **28**, 299 (1963).

[8] B. W. Lee, Phys. Rev. Letters **12**, 83 (1964).

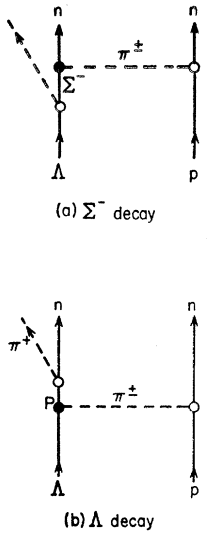

FIG. 2. One-pion exchange contributions calculated in this paper but found relatively unimportant: (a) Σ^- decay diagrams; (b) virtual $\Lambda \to p + \pi^-$ decay diagrams.

relationship based on SU(3) R invariance and later derived from unitary symmetry without R invariance by Gell-Mann.[9] In order to obtain agreement with experiment it is necessary to assume, however, that the decay

$$\Sigma^+ \to n + \pi^+ \tag{1.3}$$

proceeds to a final relative S state of the pion and neutron in disagreement with the predictions of unitary symmetry R invariance arguments.[8,10] If this final state is found by direct measurement of the neutron polarization to be P wave, then processes other than those considered in this paper will have to be invoked.

Substantial understanding of the π^+ emitting decay (1.1) can be achieved through the simple arguments outlined below. The actual calculation will be presented in Secs. II through VII.

Only mechanisms involving pion exchange between the two baryons in the elementary process

$$\Lambda + p \to n + n + \pi^+ \tag{1.4}$$

are assumed to be important. All of the contributions involving one-pion exchange are calculated (see Figs. 1 and 2). In these diagrams time is assumed to flow upwards. We calculate the one- and two-pion exchange contributions symbolized in Fig. 1(a) by solving the associated (Λ–p, Σ^+–N) coupled channel Schrödinger equation.

Of course there are many mechanisms of different character which could conceivably contribute to the decay interaction. As illustrations we give in Fig. 3 diagrams of the same order as the pole diagrams of Fig. 2. Why do we consider only the pion exchange contributions?

Contributions

The reasons for the neglect of other contributions here are: (a) the practical reason that they involve unknown coupling constants and form factors, and (b) the fact that their contributions are of a substantially shorter range and therefore contribute less effectively to the low momentum transfer interaction (1.4) occuring in the hypernucleus. This momentum transfer is small enough so that the pion pole is either very much closer than other singularities to the physical region of the amplitude or actually in the physical region. The Σ^+–n amplitude obtained from the coupled-channel Schrödinger equation associated with Fig. 1(a) is similarly of quite long range (see Fig. 5) and has, therefore, the dominantly low-momentum-transfer components effective in (1.4).

Among the diagrams considered there are some which are more important than the others. A qualitative argument which identifies these and which will be confirmed by the calculation, takes advantage of the fact that the π^+ mesons from (1.1) observed experimentally have a very low median momentum of about 60 MeV/c—much lower than the pion momenta characteristic of free Λ and Σ decays. As a result, the centrifugal barrier effects in the relative pion-baryon coordinates lead to a strong sensitivity of the calculated rates to whether the outgoing pion is emitted at an S- or P-wave vertex. For example, if the Σ^+ decay (1.3) occurs through a P rather than an S-wave coupling, its contribution will be relatively reduced by about the square of the ratio of the median experimental π^+ momentum to the π^+ momentum in the free decay. This number is about 0.1. Looking at the diagrams in Figs. 1 and 2 and remembering that the strong pion-baryon couplings are parity conserving and, therefore, P wave, it can be seen that only these diagrams involving the Σ^+ decay (1.3) and S-wave charge exchange [Fig. 1(b)] have the possibility of simple S-wave pion emission. Indeed, these processes are those found most important in the calculation if the Σ^+ decay (1.3) is assumed S wave. If this decay is P wave the charge exchange process associated with Fig. 1(b) dominates and $\pi^+/\pi^- \approx 0.004$.

It will be seen in the later sections that we are fortunate in having improvements upon perturbation

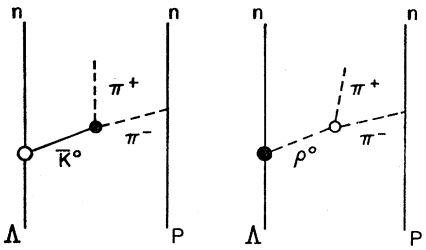

FIG. 3. Examples of contributions to π^+ hypernuclear decay not calculated in this paper.

[9] M. Gell-Mann, Phys. Rev. Letters 12, 155 (1964); see Lee and Glashow (Ref. 10) for a simple presentation of the proof.

[10] B. W. Lee and S. L. Glashow (to be published).

theoretic techniques for calculating the Σ^+ and charge exchange contributions.

Transitions

The low-momentum pions emitted in (1.1) cause only small recoils of the baryons. This makes it possible to speak, in analogy to β-decay arguments, of "allowed" and "forbidden" transitions. Because of the intrinsically two-baryon character of the interaction (1.4), the transitions are between two-baryon relative orbital states rather than single-baryon states, but the convenience is the same; it is possible to determine the spin dependence of the terms in the interaction operator which contribute predominantly to the decay. This knowledge will be used in the interpretation of our results.

Relative to the scale of the hypernucleus, almost all the interaction operators associated with the diagrams in Figs. 1 and 2 are sufficiently short ranged so that the Λ and proton can be assumed to interact in an initial S state. An exception is the interaction operator in Fig. 1(b) which has a $1/r$ dependence. For the S-shell hypernucleus ${}_\Lambda\mathrm{He}^4$, our argument will work even for this diagram, however. In atomic notation, the initial relative Λ–P state in (1.4) is thus either ${}^1S_0$ or ${}^3S_1$. Since recoil effects may be ignored, angular momentum conservation allows transitions to only certain final two neutron states: The total angular momentum of the two baryons is unchanged for S-wave pion emission and, by at most one unit for P-wave pion emission. Many of the remaining possible final states are forbidden by the Pauli principle; in addition the over-all parity of the final state is determined by the parity of the weak vertex. As a consequence of all these constraints we find that only the ${}^1S_0 \to {}^1S_0$ transitions are allowed for the S-wave virtual Σ^+ decay contribution. This is also the only transition allowed to contribute to the S-wave charge exchange of a neutral pion from the dominantly S-wave Λ-decay vertex. Above we found that these are the two processes not substantially suppressed by centrifugal barrier effects in the relative coordinate of the pions and baryons. Consequently, in this approximation, the initial ${}^3S_1$ Λ–p state cannot be expected to contribute greatly, and the dominant character of the interaction (1.4) in the hypernucleus is of a ${}^1S_0 \to {}^1S_0$ transition. We now go on to show that qualitative understanding of the observed π^+ energy spectrum may be obtained from similarly simple arguments.

π^+ Energy

In many of the experimental references, it has been noted that the pion energies from the decay (1.1) are apparently considerably lower than those from the mirror decay (1.2). (A spectrum of the published π^+ events and a typical spectrum of π^- events are presented in Fig. 4.) This has been cited as evidence supporting a particular model[11] for (1.1) in which Pauli suppression effects were ignored. We show now that, in fact, it is these effects which provide the most plausible explanation of the difference in the energy spectra.

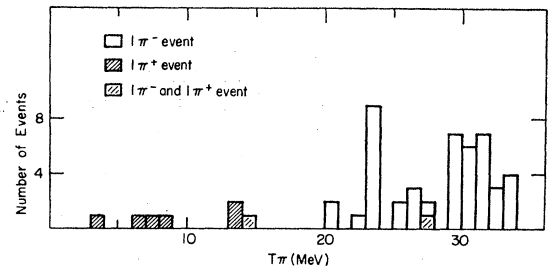

FIG. 4. π^+ and π^- energy spectra from ${}_\Lambda\mathrm{He}^4$ decays. The π^+ spectrum includes the eight events referred to in this paper (Refs. 1–7) and the π^- spectrum represents 47 uniquely identified events assembled by the EFINS emulsion group (private communication).

Crudely, ${}_\Lambda\mathrm{He}^4$ can be thought of as an He^3 core nucleus to which a Λ is loosely bound. This description seems reasonable since the energy necessary to dissociate a nucleon from He^4 is about 8 MeV compared to the 2.33 MeV necessary for the removal of the Λ. The low Λ binding energy implies that, in this and other light hypernuclei, the Λ wave function has a large tail outside of the core nucleus to which it is bound. The Λ exists, then, in two environments—it is found with about equal probability inside the He^3 core and in a region outside the radius of this core. The mechanism underlying the decay (1.1) must involve, however, at least two baryons. The Λ must therefore be in the core near a proton in order for (1.1) to occur and the final neutrons will be produced into the core environment containing another neutron. The Pauli principle requires them to be produced in states for which at least one of the neutrons has a wave function orthogonal to this spectator neutron—a state with considerably greater kinetic energy. If the neutrons are in a relative ${}^1S_0$ state, spatially symmetric in their coordinates, both must have space wave function orthogonal to that of this spectator neutron. But single-particle excitations within the He^3 radius require energies of the order of 20 MeV; therefore, little energy will be left to the π^+, since the Q value of the interaction (1.4) is only 35 MeV. In contrast, for the decay (1.2) and the decay

$$ {}_\Lambda\mathrm{He}^4 \to (\text{nucleons}) + \pi^0 , $$

the predominant mechanisms are probably the simple pionic decays of the bound Λ:

$$ \Lambda \to p + \pi^- $$
$$ \to n + \pi^0 . $$

Because the Pauli suppression effect is so strong inside the core nucleus, these decays probably occur mostly

[11] A. Deloff, J. Szymanski, and J. Wrsecionko, Bull. Acad. Polon. Sci., Ser. Sci. Math., Astron. Phys. 7, 521 (1959).

in the tail of the Λ wave function.[12] Such decays are almost free decays, and the spread of the observed π^- momentum peak is therefore due mostly to the Fermi motion of the decaying Λ. The high energy of the emitted π^- mesons (see Fig. 4) is simply due to the fact that the π^- is the light body in two-body decay and there is no other degree of freedom, as in (1.4), into which the energy release can be absorbed. It is interesting to note that, if the π^+ emission could occur from outside the region of Pauli suppression, as can the π^- emission, the branching ratio between (1.1) and (1.2) would be considerably higher than it is found to be.

Mesonic Corrections

The picture according to which π^+ and π^- emissions occur from different regions of the hypernucleus sheds light upon yet another question—that of the magnitude of mesonic corrections to π^- and π^0 decay rates of this and other light hypernuclei. The observed π^+/π^- ${}_\Lambda He^4$ decay branching ratio suggests that the amplitudes associated with mesonic corrections to π^- and π^0 emitting decays are likely to be $\sim 15\%$ of the amplitude due to free decay of the bound Λ. Thus the interference effects between the free decay and the mesonic correction terms could be as large as 30% of the main term. Experimentally it is not yet clear whether such large deviations from the impulse approximation results do occur in hypernuclear lifetimes and decay branching ratios.[13] However, the fact that the free and stimulated decay amplitudes are characteristically associated with different regions of the hypernucleus would lead us to believe that the interference terms are unlikely to be so large.[14]

The quantitative calculation and the dependence of the results upon various coupling constants and assumptions will be the subject of Secs. IV through VII. In the next section we review first the experimental work which has been done to date on the problem of π^+ emission by hypernuclei and, in Sec. III, we review the previous theoretical work.

II. EXPERIMENTAL INFORMATION

π^+ emitting hypernuclear decays have been observed following K^- capture reactions in emulsion[1–6,15–17] and helium bubble chamber[7] experiments. Eight of the observed decays have been uniquely identified as examples of (1.1) while each of the remaining two events has several interpretations.[18] It was the unique availability of data for the ${}_\Lambda He^4$ decays which determined our choice of it as the subject of detailed calculations. General considerations upon the π^+ decays of other hypernuclei are taken up in Sec. VIII.

Final Nuclear State

It would be of interest to obtain experimentally the branching ratios for the modes

$$ {}_\Lambda He^4 \rightarrow T+n+\pi^+, \tag{2.1a}$$

$$ \rightarrow D+n+n+\pi^+, \tag{2.1b}$$

$$ \rightarrow p+n+n+n+\pi^+. \tag{2.1c}$$

Unfortunately, because all modes have only two visible tracks, of the published examples of (1.1), only two have identifiable final nuclear states [(2.1a)[4] and (2.1c)[3]]. In Appendix A it is pointed out that, with the energy resolution at present achieved in emulsion and helium bubble chamber work, the determination of the branching ratios is possible only through the statistical analysis of phase-space distributions. This requires a greatly increased number of events.

π^+ Energy

A π^+ energy spectrum assembled from the published events is displayed in Fig. 4. The qualitative reasons for the low π^+ energies have been discussed in Sec. I.

Partial π^+ Decay Rate

The π^+/π^- branching ratio in ${}_\Lambda He^4$ decay gives a measure of the π^+ decay rate, since a fairly reliable estimate of the absolute π^- decay rate is obtainable for light hypernuclei such as ${}_\Lambda He^4$ using the impulse approximation and the known free Λ decay parameters.[13,19,20] A variety of observational biases must be corrected for before experimental π^+/π^- branching ratios can be quoted, however.

In emulsion the main difficulty lies in the fact that a

[12] Our division of the hypernucleus into regions in which different amounts of Pauli suppression occur is a semiclassical one and has qualitative validity in this case because the wavelengths/2π of the final outgoing nucleons are characteristically shorter than the sizes of the hypernuclear regions. The interactions are short range enough not to destroy this division.

[13] The most recent comparison of experiment with the impulse approximation has been made by R. H. Dalitz and G. Rajasekaran, Phys. Letters 1, 58 (1962).

[14] It has been pointed out to the author by R. H. Dalitz (private communication) that the two terms might in addition have substantially different spin dependences. This would further reduce the interference term contribution to the total rates.

[15] J. Schneps, Phys. Rev. 112, 1335 (1958).

[16] M. Blau, C. Carter, and A. Perlmutter, Nuovo Cimento 27, 774 (1963).

[17] D. T. Goodhead, A. Z. M. Ismail, S. Lokanathan, and Y. Prakash, Nuovo Cimento 32, 1445 (1964).

[18] Two events (Refs. 15, 17) have interpretations as ${}_\Lambda Be^7 \rightarrow Li^6+n+\pi^+$ or ${}_\Lambda Li^7 \rightarrow He^6+n+\pi^+$. Schneps' event might also be the decay of a higher isotope of one of these hypernuclei giving off more free neutrons in the final state. The event of Blau *et al.* (Ref. 16) might be the π^+ decay of ${}_\Lambda H^3$ or ${}_\Lambda H^4$.

[19] The calculation of R. H. Dalitz and L. Liu, Phys. Rev. 116, 1312 (1959), gives the decay rate

$$\Gamma({}_\Lambda He^4 \rightarrow \text{nucleons}+\pi^-) = 1.1\times 10^{10}/\text{sec},$$

using the Λ decay rate obtained by Block *et al.* [M. M. Block, R. Gessaroli, S. Ratti, L. Grimellini, T. Kikuchi, L. Lendinara, L. Monari, E. Harth, W. Bugg, and H. Cohn, Phys. Rev. 130, 766 (1963)]

$$\Gamma_\Lambda = 4.25\times 10^9/\text{sec},$$

and an S/P amplitude ratio consistent with that obtained by Humphrey and Ross (Ref. 20).

[20] W. Humphrey and R. R. Ross, Phys. Rev. 127, 1305 (1962)

large number of π^- ${}_\Lambda He^4$ decays have been observed but not reported. There is also a large class of ambiguous ${}_\Lambda$He decays which have such short recoil tracks that it is impossible to distinguish He^3 from He^4 recoils and, therefore, ${}_\Lambda He^4$ decays from the more common ${}_\Lambda He^5$ decays. A statistical separation on the basis of observed Q values for the decays is possible in principle but not entirely free from systematic error since the percentage of events interpreted as ambiguous varies greatly for different experimental groups. The EFINS emulsion group has made corrections to these biases as carefully as is possible at the present time and obtain the estimate of 219 π^- ${}_\Lambda He^4$ decay events so far observed in emulsion.[6] The π^+/π^- branching ratio observed in emulsion is therefore $6/219=(2.7\pm1.1)\%$, where only statistical error is indicated.

The experimental errors in the helium bubble chamber are smaller but so, unfortunately, are the statistics obtained so far. Corrections affect π^+ and π^- emitting decays proportionately so that the observed ratio $2.5/78=(3\pm2)\%$ may be used directly.[7] (The 0.5 π^+ event corresponds to an event which is also interpretable as an unusual nonmesonic decay.)

The two experimental ratios obtained above are consistent within statistics and give the combined ratio

$$R_{\rm exp}\left(\frac{{}_\Lambda He^4 \to \pi^+ + (\text{nucleons})}{{}_\Lambda He^4 \to \pi^- + (\text{nucleons})}\right) = (2.9\pm1)\%, \quad (2.2)$$

where again only statistical error is quoted.

III. PREVIOUS THEORETICAL APPROACHES

Calculations have previously been attempted of the contributions associated with the two mechanisms represented in Fig. 1: (a) π^+ decay of a virtual Σ^+–n state to which the Λ–p pairs are thought to be strongly coupled,[11,21,22] and (b) a preliminary calculation has been made of the contribution of charge exchange of an outgoing π^0 from neutral Λ decay.[23] Since these are the mechanisms which are found to be dominant in our model, we explain here briefly its great difference from the earlier works.

The calculation by Deloff *et al.*[11] considers ${}_\Lambda He^4$ as a Λ–He^3 system coupled to a Σ^+–H^3 system. The structure of the core nucleus is ignored and, therefore, also the possibility of breakup and the consequent Pauli suppression effects which we find in our calculation to have order of magnitude effects. They calculate the coupling by purely static approximation perturbation theory, an approximation which has first been found inapplicable to the Λ–N, Σ–N coupling by Lichtenberg and Ross[24] in an early binding energy calculation. Finally, the order of magnitude effect which we find depends upon the S- or P-wave nature of the Σ^+ decay has not been found by these authors; however, we cannot quote definite rates from their calculation because of inconsistencies resulting from misprints in their paper.

Iwao's argument[21] is based upon the assumption that the amplitude of the Σ^+ component and therefore its contribution to the Λ-nucleus interaction depends primarily upon the isotopic spin of the core nucleus. An implicit assumption is that the core nucleus wave function must remain in its ground state when the Λ is in a Σ^+ state. This is a doubtful assumption, however, since the virtual Σ^+ energy level is already at 75 MeV, a large energy in comparison to the core nucleus level spacings, and the Λ–N interaction is quite short ranged and, therefore, quite able to cause transitions. After making this assumption, Iwao then makes an interesting attempt to relate the Σ^+ state amplitude to the variation of the P-shell hypernuclear binding energies, but the accuracy of the measured binding energies turns out to be inadequate for any concrete prediction.

Biswas argues[22] that the π^- decay of a hypernucleus occurs predominantly through higher order diagrams than are involved in the simple decay of a bound Λ, on the grounds that the lowest order diagram in nonmesonic decay does not give the experimental neutron to proton stimulation ratio. This ignores the fact that impulse approximation calculations do correspond rather well with the experimental facts in π^- and π^0 decays[13] and that very much larger momentum transfers are involved in the nonmesonic decay. In Biswas' argument the small π^-/π^0 ratio observed is essentially attributed to the divergence of the perturbation series in strong interactions, the π^- mode being assumed due to higher order diagrams than the π^+ mode.

Dalitz and von Hippel have considered in a preliminary calculation the contributions of the S-wave charge exchange mechanism [see Fig. 1(b)] to (1.1) in the completeness approximation. For an assumed final π^+ energy of about 10 MeV (see Fig. 4) they obtained a ${}_\Lambda He^4$ π^+/π^- decay branching ratio of about 0.4%.[23] When a hard core is introduced into the baryon-baryon potential the rate drops to about 0.25%, so that it appears that charge exchange scattering by itself cannot explain the observed branching ratio.

In the next two sections we outline the procedures used to obtain the interaction operators associated with the processes in Figs. 1 and 2. Those contributions for which static approximation results are thought to be adequate are calculated in Sec. IV. In Sec. V we take up the contributions associated with Fig. 1(a) for which it is necessary to solve a coupled-channel Schrödinger equation.

[21] S. Iwao, Nuovo Cimento **25**, 890 (1962).
[22] N. N. Biswas, Nuovo Cimento **28**, 1527 (1963).
[23] R. H. Dalitz and F. von Hippel, Nuovo Cimento (to be published).
[24] D. B. Lichtenberg and M. H. Ross, Phys. Rev. **107**, 1714 (1957).

IV. INTERACTION OPERATORS CALCULATED IN STATIC APPROXIMATION WEAK VERTICES

We take the general form of the weak baryon-pion vertex, $B \to B'+\pi$, to be of the static form

$$H_w(\mathbf{x}) = f_w \bar{B}'\left(S+\frac{P(\boldsymbol{\sigma}\cdot\mathbf{q})}{q_f}\right)\phi(\mathbf{x})B\,, \qquad (4.1)$$

where $|S|^2+|P|^2=1$, q is the momentum of the pion, q_f its momentum for the free decay, $\bar{B}'$ and B are, respectively, creation and annihilation operators, and $\boldsymbol{\sigma}$ is the vector of Pauli spin matrices. The diagrams which we consider in Figs. 1 and 2 contain the following weak amplitudes (we use Lee's notation[8]):

$$A(\Lambda_-{}^0) \equiv A(\Lambda \to p+\pi^-)\,, \qquad (4.2a)$$

$$A(\Lambda_0{}^0) \equiv A(\Lambda \to n+\pi^0)\,, \qquad (4.2b)$$

$$A(\Sigma_+{}^+) \equiv A(\Sigma^+ \to n+\pi^+)\,, \qquad (4.2c)$$

$$A(\Sigma_-{}^-) \equiv A(\Sigma^- \to n+\pi^-)\,. \qquad (4.2d)$$

Enough experimental data are available for these decays to restrict considerably the associated f_w, S, and P: The decay rates fix the magnitude of the f_w and the parameters α,

$$\alpha = 2\,\mathrm{Re}(SP)\,, \qquad (4.3)$$

describing the asymmetry of the final pion momentum distribution relative to hyperon polarization in the hyperon decay frame as $1+\alpha\hat{q}\cdot\hat{P}$, restricting S and P to two sets of values if their small imaginary components are ignored. In addition, polarization measurements on the final proton and the experimental branching ratios to final nuclear states in ${}_\Lambda\mathrm{He}^4$ π^- decay fix the set of S, P for (4.2a) as that dominantly S wave.[25]

The remaining ambiguities are the relative signs of the decay interactions (which are experimentally unknown because they have physical consequences only in the interference of virtual processes such as those in Fig. 1) and the choice from the two sets of values for S, P associated with (4.2b), (4.2c), and (4.2d). A convincing approximate higher symmetry scheme for the weak interactions may soon resolve these ambiguities theoretically, however. The $|\Delta I| = \frac{1}{2}$ rule will probably be a component of such a scheme[26] and predicts

$$A(\Lambda_-{}^0) = -\sqrt{2}A(\Lambda_0{}^0)\,, \qquad (4.3a)$$

$$A(\Sigma_0{}^+) = (1/\sqrt{2})[A(\Sigma_+{}^+) - A(\Sigma_-{}^-)], \qquad (4.3b)$$

where

$$A(\Sigma_0{}^+) = A(\Sigma^+ \to p+\pi^0)\,.$$

This rule fits naturally into Cabibbo's proposed[27] unitary symmetry scheme in which the strangeness changing nonleptonic decay interaction transforms as a member of an octet. Gell-Mann has shown[9] that there are only three independent ways in which a CP-invariant parity-violating interaction operator may be constructed to transform in this way. There is consequently a constraint upon the S-wave components of the four independent observable baryon nonleptonic decay amplitudes remaining after the application of the $|\Delta I| = \frac{1}{2}$ rule, giving the constraint[28]

$$A_s(\Xi_-{}^-) = -(1/\sqrt{2})\{A_s(\Lambda_0{}^0) + (\sqrt{3}/2) \times [A_s(\Sigma_+{}^+) - A_s(\Sigma_-{}^-)]\}\,, \qquad (4.4)$$

where

$$A_s(\Xi_-{}^-) = A_s(\Xi^- \to \Lambda+\pi^-)\,.$$

The analysis of Lee[8] shows that this relationship is compatible with the magnitudes of A, obtained experimentally and is, in fact, reasonably satisfied by the magnitudes of the P-wave amplitudes as well. He has derived the relationship

$$A(\Xi_-{}^-) = -(1/\sqrt{2})\{A(\Lambda_0{}^0) + (\sqrt{3}/2) \times [A(\Sigma_-{}^-) - A(\Sigma_+{}^+)]. \qquad (4.5)$$

From SU(3)R invariance, his argument would also require the $\Sigma^+ \to n+\pi^+$ decay to be P-wave, however, in which case our model fails to work. Our model only works if $\Sigma^+ \to n+\pi^+$ is S-wave and the relative phases of $A_s(\Lambda_0{}^0)$ and $A_s(\Sigma_+{}^+)$ then required by Eqs. (4.4), (4.3b), and experiment hold.

The experimentally small asymmetry parameters of (4.2c) and (4.2d) (compatible with zero[25]) along with the $|\Delta I| = \frac{1}{2}$ rule in the form (4.3b) gives the alternative sets of S and P associated with $A(\Sigma_-{}^-)$ and $A(\Sigma_+{}^+)$:

$$S(\Sigma_+{}^+) = P(\Sigma_-{}^-) \approx \pm 1\,, \quad P(\Sigma_+{}^+) = S(\Sigma_-{}^-) \approx 0 \qquad (4.6a)$$

or

$$P(\Sigma_+{}^+) = S(\Sigma_-{}^-) \approx \pm 1\,, \quad S(\Sigma_+{}^+) = P(\Sigma_-{}^-) \approx 0\,. \qquad (4.6b)$$

Depending upon which alternative is taken, when these choices are substituted in Eq. (4.5) the relative signs of $A(\Lambda_0{}^0)$ and $A(\Sigma_{+(-)}{}^{+(-)})$ are fixed. If then we adopt a convention in which the weak coupling constants and $S(\Lambda_0{}^0)$ are all assumed positive, Eqs. (4.6) reduces to two sets of S and P depending upon whether the $\Sigma^+ \to n+\pi^+$ decay is S wave,

$$S(\Sigma_+{}^+) = P(\Sigma_-{}^-) = +1\,, \quad P(\Sigma_+{}^+) = S(\Sigma_-{}^-) \approx 0 \qquad (4.7a)$$

or P wave,

$$P(\Sigma_+{}^+) = S(\Sigma_-{}^-) = +1\,, \quad S(\Sigma_+{}^+) = P(\Sigma_-{}^-) \approx 0\,. \qquad (4.7b)$$

The Λ channel parameters are completely fixed by

[25] For review discussions of the experimental status of the hyperon pionic decay parameters see R. H. Dalitz [Proceedings of the 1963 Brookhaven Conference on Weak Interactions (to be published)] and also F. C. Crawford, in *Proceedings of the 1962 Annual International Conference on High-Energy Physics at CERN*, edited by J. Prentki (CERN Scientific Information Service, Geneva, 1962), p. 827.

[26] See R. H. Dalitz (Ref. 25) for a review of the current experimental status of this rule.

[27] N. Cabibbo, Phys. Rev. Letters **12**, 62 (1964).

[28] Here we adopt the convention used by J. J. de Swart, Rev. Mod. Phys. **35**, 916 (1963), where the relative phases of the baryon fields are fixed by requiring all the elements of the I_+, K_+ matrices be positive.

(4.3a) and experiment[29] as

$$S(\Lambda_0^0) = -S(\Lambda_-^0) = 0.944, \qquad P(\Lambda_0^0) = -P(\Lambda_-^0) = 0.328. \tag{4.8}$$

The coupling constants are fixed by (4.3) and experiment[30] as,

$$\frac{f^2(\Lambda_-^0)}{4\pi} = \frac{2f^2(\Lambda_0^0)}{4\pi} = 1\times 10^{-14}, \qquad \frac{f^2(\Sigma_+^+)}{4\pi} = \frac{f^2(\Sigma_-^-)}{4\pi} = 1.37\times 10^{-14}. \tag{4.9}$$

Strong Vertices

The relative $(\Sigma\Lambda\pi)$ parity is now well known to be negative[31] with the consequence that all of the strong vertex couplings in Figs. 1 and 2 must be either pseudoscalar or pseudovector. The general static form of the strong vertices is then[28]

$$H_s(\mathbf{x}) = [f_{NN\pi}\bar{N}_\alpha(\tau_i)_{\alpha\beta}(\boldsymbol{\sigma}\cdot\mathbf{q})N_\beta\delta_{ik} + f_{\Sigma\Lambda\pi}(\bar{\Sigma}_i(\boldsymbol{\sigma}\cdot\mathbf{q})\Lambda + \bar{\Lambda}(\boldsymbol{\sigma}\cdot\mathbf{q})\Sigma_i)\delta_{ik} - if_{\Sigma\Sigma\pi}\bar{\Sigma}_i(\boldsymbol{\sigma}\cdot\mathbf{q})\Sigma_j\epsilon_{ijk}]\phi_k(\mathbf{x}), \tag{4.10}$$

where ijk are all isospin indices, δ_{ik} is the Krönecker δ function, ϵ_{ijk} is $(-)^P$, where P is the order of the permutation of ijk, $(\tau_i)_{\alpha\beta}$ are the Pauli isospin matrices, $\bar{N}_\alpha$, N_β, $\bar{\Sigma}_i$, Σ_i, $\bar{\Lambda}$, and Λ are the creation and annihilation operators of the baryons, $\phi_k(\mathbf{x})$ is a component of the pion field isospin vector.

$f_{NN\pi}{}^2/4\pi$ is well known from π–N forward scattering dispersion relations[32] to be 0.081 ± 0.003. $f_{\Sigma\Lambda\pi}{}^2/4\pi$ and $f_{\Sigma\Sigma\pi}{}^2/4\pi$ have been estimated in two ways:

(a) Fitting the predictions of theoretical pionic exchange potentials to the Λ–n scattering lengths obtained from hypernuclear binding energy systematics and to the experimental branching ratio at rest $R(\Sigma^-+p) \to (\Sigma^0+n)/(\Lambda+n)$ gives[33] $f_{\Sigma\Lambda\pi} \approx f_{NN\pi}$ and $f_{\Sigma\Sigma\pi} \leq \frac{1}{2} f_{NN\pi}$.

(b) Crude unitary symmetry calculations of the positions and partial widths of the $P_{3/2}$ baryon-pion decuplet bootstrapped with the baryon octet appear to achieve self-consistency and rough consistency with experiment for the D–F mixing parameter in the baryon-pseudoscalar couplings, $\alpha_P \approx \frac{1}{4}$,[34] giving $f_{\Sigma\Lambda\pi} \approx 0.70 f_{NN\pi}$, $f_{\Sigma\Sigma\pi} \approx 0.39 f_{NN\pi}$. The fact that such different approaches lead to similar conclusions is encouraging and in Sec. VII we choose the results for the unitary symmetry coupling constants associated with $\alpha_P = \frac{1}{4}$ (D/F mixing ratio $= 3$) for the most detailed comparison with experiment.

Perturbation Operators

The diagrams calculated strictly according to static perturbation theory are those given in Fig. 2 which, according to the qualitative arguments of Sec. I confirmed by the numerical results of Sec. VII, are unimportant. The associated interaction operators are written out in Appendix B, where the evaluation of the integrals is also discussed.

Charge Exchange Contribution

The π^0 pole contribution to (1.1) [see Fig. 1(b)] gives an interaction operator proportional to $\exp(iq_0 r)/r$, where $\mathbf{q}_0$ is the momentum of the exchanged π^0 on its mass shell. In the static model[34]

$$q_0{}^2 = (M_\Lambda - M_n)^2 - 1$$

but, since this number is quite small, it will be affected by recoil terms and, in the actual calculation, we test the dependence of our results upon this parameter. The low-energy pion-nucleon phase shifts may then be used to obtain the interaction operator[35]

$$\{f(\Lambda_0^0)S(\Lambda_0^0)/(16\pi^3\omega_q)^{1/2}\} \times\{a_{CE}{}^1 + [2i(\mathbf{q}\cdot\hat{r}) + \boldsymbol{\sigma}_p\cdot(\mathbf{q}\times\hat{r})][(1/r) - iq_0]a_{CE}{}^3\} \times\{\exp(iq_0 r)/r\}\exp(-i\mathbf{q}\cdot\mathbf{r}_p), \tag{4.11}$$

where $\mathbf{q}_0$ and $\mathbf{q}$ are, respectively, the momenta of the exchanged and final pions and $\mathbf{r} = \mathbf{r}_p - \mathbf{r}_\Lambda$. $a_{CE}{}^1$ and $a_{CE}{}^3$ may be interpreted as the S- and P-wave charge exchange scattering lengths[36]

$$a_{CE}(\pi^0 p \to \pi^+ n) = \tfrac{1}{3}\sqrt{2}[a(T=\tfrac{3}{2}) - a(T=\tfrac{1}{2})] \tag{4.11a}$$

$$a_{CE}{}^1 = -0.122\mu^{-1}, \quad a_{CE}{}^3 = 0.115\mu^{-3}. \tag{4.11b}$$

The P-wave term in Eq. (4.11) becomes quite singular toward the origin, and in Appendix B, cutoff-dependent terms cancelling some of this behavior are introduced in an effort to make the completeness approximation used in Sec. VI more realistic. Our conclusions are independent of this cutoff up to very high values, however.

V. COUPLED-CHANNEL SCHRÖDINGER EQUATION FOR VIRTUAL Σ^+–n AMPLITUDE

The interaction operator for the diagrams represented in Fig. 1(a) is proportional to the amplitude of

[29] See Ref. 25. $P^2(\Lambda)$ is so small and its effect so reduced in our process by centrifugal barrier effects that, in the actual calculation, it has been taken as zero.

[30] Using the lifetimes $\tau_\Lambda = 2.36\times 10^{-10}$/sec and $\tau_{\Sigma^-} = 1.58\times 10^{-10}$/sec obtained, respectively, by Block *et al.* (Ref. 19) and Humphrey and Ross (Ref. 20) with branching ratio (Ref. 20) $R(\Sigma^+ \to p\pi^0/n\pi^+) \approx 1$.

[31] M. B. Watson, M. Ferro-Luzzi, and R. D. Tripp, Phys. Rev. **131**, 2248 (1963).

[32] J. Hamilton and W. S. Woolcock, Rev. Mod. Phys. **35**, 737 (1963).

[33] J. J. de Swart and C. K. Iddings, Phys. Rev. **128**, 2810 (1962); **130**, 319 (1963).

[34] R. E. Cutkosky, Ann. Phys. (N. Y.) **23**, 415 (1963); A. W. Martin and K. C. Wali, Phys. Rev. **130**, 2455 (1963); and to be published.

[35] $P(\Lambda)$ has been taken equal to zero here (see Footnote 29) and the P-wave π-N scattering is approximated as occurring in the $J = \frac{3}{2}$ state.

[36] See Ref. 32. As the S-wave scattering is zero in static approximation but in fact dominates for the scattering energies in (1.1), this is a particularly important improvement over the perturbation theoretic approach.

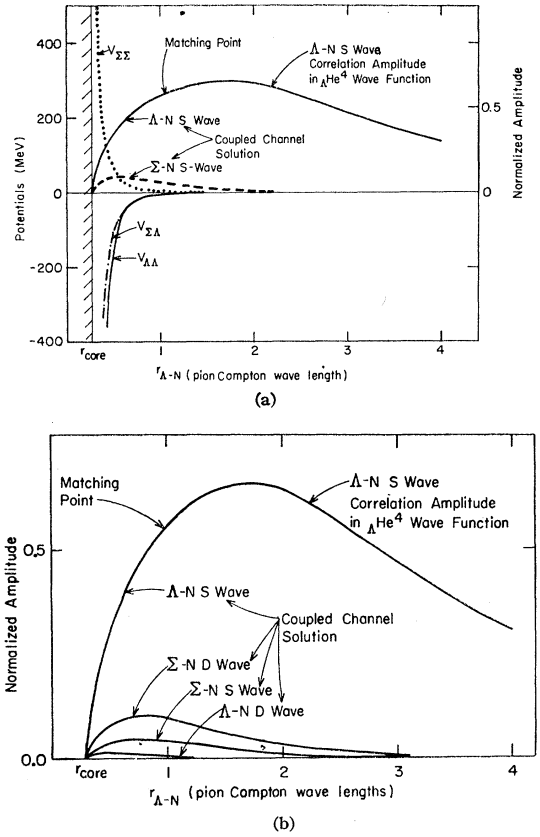

FIG. 5. The $\Lambda-N$ correlation wave function (times $r_{\Lambda N}$) in ${}_{\Lambda}\mathrm{He}^4$ calculated for the unitary symmetry mixing parameter $\alpha_p=\frac{1}{4}$, $r_s=0.26$, $r_T=0.28$: (a) $J=S=0$ components and the potentials (Ref. 33a) de Swart and Iddings used in their calculation; (b) $J=S=1$ components.

the Σ^+–n component of the wavefunction in the Λ–p relative coordinate. We calculate this amplitude using the coupled-channel Schrödinger equation computer program and theoretic mesonic exchange potentials of de Swart and Iddings.[33] Lichtenberg and Ross first suggested[23] in 1957 that such an approach will give a great improvement over perturbation theory for the contribution of the low-lying Λ–N state to the Σ–N potential. The advantage is apparent from Fig. 5(a) where the radial dependence of the $J=S=0$ component of this amplitude may be compared to that of the potentials to which it would be proportional (except for a factor $r_{\Lambda-N}$) in lowest order perturbation theory. It can be seen that the wave function has a much longer tail than the potentials because of the low energy of the Σ–N virtual state. Also unitarity prevents the Σ–N component from being as singular toward the origin as are the potentials, with the consequent practical advantage that the virtual Σ–N component becomes less dependent than in perturbation theory upon the poorly understood short-range contributions to the interaction. In fact, we find that variations of the hard-core radius which affect, for instance, the hypernuclear binding energies by many MeV affect the Σ–N amplitudes only slightly.

Aside from spin and centrifugal barrier effects, the two-channel Schrödinger equation assumes the matrix form:

$$\left[-\underbrace{\begin{pmatrix}1/2M_\Lambda & 0\\ 0 & 1/2M_\Sigma\end{pmatrix}}_{\text{reduced masses}}\nabla^2 + \begin{pmatrix}V_{\Lambda\Lambda}(r) & V_{\Lambda\Sigma}(r)\\ V_{\Sigma\Lambda}(r) & V_{\Sigma\Sigma}(r)\end{pmatrix}-\begin{pmatrix}E & 0\\ 0 & E+M_\Sigma-M_\Lambda\end{pmatrix}\right] \times\begin{pmatrix}\psi_{\Lambda N}(r)\\ \psi_{\Sigma N}(r)\end{pmatrix}=\begin{pmatrix}0\\ 0\end{pmatrix}. \quad (5.1)$$

$V_{\Lambda\Lambda}$, $V_{\Sigma\Lambda}$, $V_{\Lambda\Sigma}$, and $V_{\Sigma\Sigma}$ symbolize with spin indices suppressed the static potentials associated with the interactions $\Lambda+N\rightarrow\Lambda+N$, $\Sigma+N\rightarrow\Lambda+N$, $\Lambda+N\rightarrow\Sigma+N$, and $\Sigma+N\rightarrow\Sigma+N$ for total isotopic spin-$\frac{1}{2}$ states. The physical solution of this wave equation obeys the boundary conditions that it go to zero at the phenomenological hard-core radius and that $\psi_{\Lambda N}(r)$ and $\psi_{\Sigma N}(r)$ have, respectively, the characteristics of a positive energy scattering state and a bound state for large separations r.

De Swart and Iddings modeled their calculations of the potentials upon the reasonably successful calculations made by Brueckner and Watson[37] in an early model of the nucleon-nucleon potentials. Their potentials depend on the pion-baryon coupling constants, $f_{NN\pi}$, $f_{\Sigma\Sigma\pi}$, $f_{\Sigma\Lambda\pi}$ discussed in the last section and upon assumed hard-core radii in the singlet and triplet relative spin states. The strongly singular nature of the potentials requires some cutoff and the experimental evidence for a hard core in the nucleon along with suggestive similarities in the interactions of the baryons make it a reasonable conjecture that hard cores might exist in all baryon-pion interactions. This point of view has been elegantly formulated by Kalckar[38] in a model in which a strongly coupled unitary singlet vector meson produces a hard core in all baryon-baryon interactions, the radius of which varies somewhat because of effects associated with the more weakly coupled unitary octet of vector mesons. In accord with such a picture, de Swart and Iddings considered only hard-core radii close to those ($\approx$0.5 F) observed in nucleon-nucleon scattering. This assumption makes up in part for their lack of an explicit treatment of vector meson exchange terms which have been found important in recent nucleon-nucleon potentials.[39]

The spin dependence of the hard-core radius and the

[37] K. A. Brueckner and M. B. Watson, Phys. Rev. **92**, 1023 (1953).
[38] J. Kalckar, Phys. Rev. **131**, 2242 (1963).
[39] See, e.g., A. Scotti and D. Y. Wong, Phys. Rev. Letters **10**, 142 (1963).

coupling constants $f_{\Sigma\Lambda\pi}$ and $f_{\Sigma\Sigma\pi}$ were varied in de Swart and Iddings' calculations until sets of values giving the Λ–N S-wave scattering lengths and $\Sigma^+ + p \to (\Sigma^0+n/\Lambda+n)$ capture ratios were obtained. In Fig. 5 we give the S-wave dominant solutions for one of these sets, matched to the normalized S-wave Λ–p amplitude of the variational correlation wavefunction in the ${}_\Lambda He^4$ nucleus (see Sec. VI). The matching has been made at a separation of one-pion Compton wavelength, a natural boundary for the interaction region which may be varied within reasonable limits without large effects, as may be seen in the figure from the continuity of the derivative and curvature at the matching point. For the triplet spin relative wave function, the tensor interactions introduce D-wave components, as may be seen in Fig. 5(b). The interaction operator associated with the virtual Σ^+ decay process of Fig. 1(a) will then be

$$-(\tfrac{2}{3})^{1/2}[f(\Sigma_+{}^+)/(16\pi^3\omega_q)^{1/2}]\bar{N}[S(\Sigma_+{}^+)+P(\Sigma_+{}^+)(\boldsymbol{\sigma}_\Lambda\cdot\mathbf{q})/q_\Sigma][{}^1S_0(r){}^1\mathbf{\Pi}_{\Lambda p}+{}^3S_1(r){}^3\mathbf{\Pi}_{\Lambda p}+(9/8)^{1/2}\,{}^3D_1(r)\mathbf{T}_{\Lambda p}(\hat{r})]\Lambda, \quad (5.2)$$

where ${}^1S_0$, ${}^3S_1$, and ${}^3D_1$ are, respectively, the singlet S, triplet S, and D-wave Σ–N amplitudes in the Λ–p relative coordinate; ${}^1\mathbf{\Pi}_{\Lambda p}$ and ${}^3\mathbf{\Pi}_{\Lambda p}$ are singlet and triplet spin projection operators,

$$\mathbf{T}_{\Lambda p}=(\boldsymbol{\sigma}_\Lambda\cdot\hat{r})(\boldsymbol{\sigma}_p\cdot\hat{r})-\tfrac{1}{3}(\boldsymbol{\sigma}_\Lambda\cdot\boldsymbol{\sigma}_p)$$

and the coefficient $-(\frac{2}{3})^{1/2}$ in Eq. (5.2) is the Clebsch-Gordan coefficient for the Σ^+–n component in the $T=\frac{1}{2}$, $T_z=\frac{1}{2}$ Σ–N system.

VI. THE DECAY OF ${}_\Lambda He^4$

The matrix element for ${}_\Lambda He^4$ π^+ decay to a final nuclear state $\psi_f(3n,p)$ may be written:

$$M_{fi}(E_f,\mathbf{q})=\langle\psi_f(3n,p),\pi^+(\mathbf{q})\,|\,\bar{n}(r_\Lambda)\bar{n}(r_p)\times[\bar{\phi}(\mathbf{r}_\Lambda)I_\Lambda(\mathbf{r},\boldsymbol{\sigma}_\Lambda,\boldsymbol{\sigma}_p,\mathbf{q})+\bar{\phi}(\mathbf{r}_p)I_p(\mathbf{r},\boldsymbol{\sigma}_\Lambda,\boldsymbol{\sigma}_p,\mathbf{q})]\times\Lambda(\mathbf{r}_\Lambda)p(\mathbf{r}_p)\,|\,\psi_i(\Lambda;n;2p)\rangle, \quad (6.1)$$

where $\psi_i(\Lambda;n;2p)$ is the initial wave function antisymmetrized in the proton coordinates; $\bar{n}$, $\bar{\phi}$ and Λ, p are fields containing, respectively, creation operators for the final neutrons and π^+ and annihilation operators for the initial Λ and proton; I_Λ and I_p represent sum of the interaction operators separated according to whether the recoil due to the π^+ emission is taken up by the "Λ neutron" as in Fig. 1(a) or at the "p neutron" as in Fig. 1(b).

In terms of the matrix element (6.1) and the initial mass of the hypernucleus M_A, the final π^+ emission rate is then given by

$$\Gamma_+=2\pi\int d\mathbf{q}\int_{(M_{He^3}+M_N)} dE_f\rho(E_f)\,|M_{fi}(E_f,\mathbf{q})|^2\times\delta(E_f+\omega_q-M_A). \quad (6.2)$$

Upon integration over the magnitude of the pion momentum q, Eq. (6.2) becomes

$$\Gamma_+=2\pi\int d\Omega_q\int_{(M_{He^3}+M_N)}^{(M_A-M_\pi)} dE_f\rho[E_f]\rho_\pi[q(E_f)]\times|M_{fi}(\hat{q},E_f)|^2, \quad (6.3)$$

where

$$\rho_\pi[q(E_f)]=q(E_f)\omega(E_f)[1-\omega(E_f)/M_A]$$

and

$$\omega(E_f)=[q^2(E_f)+1]^{1/2}=M_A-E_f.$$

Completeness Approximation

If M_{fi} satisfies the following condition as a function of E_f, it may be possible to apply the "completeness" approximation to (6.3): $M_{fi}(E_f)^2$ must decrease sufficiently rapidly with increasing E_f so that the upper limit (M_A-m_π) in the integral over E_f in (6.3) may be removed and integral carried to infinity without greatly altering its value. If this assumption is satisfied and q is taken as a parameter to be varied within a range given by experiment, the simplification of calculation necessary to evaluate Γ_+ in Eq. (6.3) is enormous —the completeness property of the four-nucleon states $\psi_f(3n,p)$ may be used. We justify the approximation below after demonstrating its consequences.

Taking one of the four terms $I_{l'}{}^\dagger\cdot I_l$, where l, l' stand for either Λ or p, Eq. (6.3) may be expanded to show explicitly its dependence upon ψ_f. Substituting some average value $\mathbf{q}_{\rm av}$ for $\mathbf{q}(E_f)$, (6.3) then becomes

$$\Gamma_+=2\pi\rho_\pi(\mathbf{q}_{\rm av})\int d\Omega_q\langle\psi_i|\,I_{l'}{}^\dagger\exp(-i\mathbf{q}_{\rm av}\cdot\mathbf{r}_{l'})\times\left\{\int_{(M_{He^3}+M_N)}^{\infty} dE_f\rho(E_f)\,|\psi_f\rangle\langle\psi_f|\right\}\times\exp(i\mathbf{q}_{\rm av}\cdot\mathbf{r}_l)I_l|\psi_i\rangle. \quad (6.4)$$

The dependence upon E_f now lies entirely within the curly brackets and the completeness substitution may be made:

$$\int_{(M_{He^3}+M_\Lambda)}^{\infty} dE_f\rho(E_f)\psi_f(1'2'3';4)\psi_f{}^\dagger(123;4)=[1/(3!)][\textstyle\sum_{P'}(-)^{P'}\delta_{1'1}\delta_{2'2}\delta_{3'3}], \quad (6.5)$$

where 1, 2, 3: 1′, 2′, 3′ stand for the spin and space coordinates of final neutrons and 4 for the "spectator" proton.[40] The form (6.5) takes explicit account of the Pauli antisymmetrization between the three final neutrons in ψ_f; the sum is over the six permutations P'

[40] The fact that 4 is indistinguishable from the "stimulating" proton and could equally well be involved in (1.4) multiplies our final results by 2.

of the neutron indices. Equation (6.4) now becomes[41]

$$\Gamma_+=2\pi\rho_\pi(\mathbf{q}_{\rm av})\int d\Omega_q \sum_{P'}(-)^{P'}\langle\psi_i(1';2';3'4)|$$
$$\times I_{l'}{}^\dagger(\mathbf{r}_{1'3'},\boldsymbol{\sigma}_{1'},\boldsymbol{\sigma}_{3'},\mathbf{q}_{\rm av})\exp(-i\mathbf{q}_{\rm av}\cdot\mathbf{r}_{l'l})\delta_{1'1}\delta_{2'2}\delta_{3'3}$$
$$\times I_l(\mathbf{r}_{13},\boldsymbol{\sigma}_1,\boldsymbol{\sigma}_3,\mathbf{q}_{\rm av})|\psi_i(1;2;34)\rangle. \quad (6.6)$$

It is worthwhile noting that the term in the permutation summation of Eq. (6.6) for which $1'=1$, $2'=2$, $3'=3$ is just the rate which would be calculated in completeness approximation if there were no Pauli principle and the final neutrons resulting from (1.4) were distinguishable among themselves and from the "spectator" neutron. For this reason, we will call this the "classical" term and will gauge the effect of the Pauli suppression in terms of the "Pauli suppression factor," the ratio of our calculated rate to the classical term.[40]

Justification of the Completeness Approximation

The matrix element (6.1) consists of the overlap integral of final and initial nuclear wave functions multiplied by an interaction operator in the Λ–p coordinate and a recoil term due to the emission of the π^+. If the overlap with high-energy final nuclear states is poor, the completeness approximation will be satisfied. The recoil is small and the initial correlations are primarily long range so that the interaction operator is the major possible source of high Fourier terms. If we take as a typical form the Yukawa potential which has the Fourier transform

$$Y(k)=[k^2+1]^{-1},$$

$Y(k)$ will essentially determine the matrix elements to final momentum states of relative momentum k in the Λ–p coordinate. $Y(k)$ cuts off rapidly for $k>1$ or at an internal energy of the final neutron pair of about 20 MeV. Since the Q value of the ${}_\Lambda$He^4 π^+ decay is about 33.4 MeV, for this case, the completeness approximation appears reasonable.

$Y(k)$ actually has more high Fourier components than the interaction operators found most important in Sec. VII: those associated with Fig. 1(a) (see Fig. 5) and with the S-wave charge exchange scattering of Fig. 1(b); and has less high Fourier components than those operators associated with P-wave charge exchange scattering in Fig. 1(b) and the processes in Fig. 2. The estimate obtained for the first set of processes will be reasonable, therefore, but the contributions of the last processes will be overestimated in completeness approximation. When cutoffs at about $k=2.4$ are introduced in their Fourier transforms (see Appendix B), their contributions will be found to be down by an order of magnitude from those of the less singular interaction operators, however, making accuracy unnecessary. Even without cutoffs, their contributions are not sufficiently large to affect our conclusions (see Sec. I for reasons).

It is not clear that $M_{fi}(E_f)^2$ is sufficiently peaked in E_f to define unambiguously an appropriate $\mathbf{q}_{\rm av}$ as is the case in the π^- and π^0 decays of light hypernuclei discussed in Sec. I. We will, therefore, consider $\mathbf{q}_{\rm av}$ as a parameter, taking its experimental distribution as a guide in the discussion of Sec. VII.

The Initial Wave Function

The initial hypernuclear wave function is taken to have the form

$$\psi_i(1;2;3,4)=(N)^{-1/2}\phi(1;234)\chi(12;34), \quad (6.7)$$

where N is the normalization integral, χ is a product of singlet spin-wave functions of the (Λ,n) pair (1,2) and proton pair (3,4). ϕ is a spin-independent wave function in the space coordinates:

$$\phi(1;234)=F(|\mathbf{r}_1-\tfrac{1}{3}(\mathbf{r}_2+\mathbf{r}_3+\mathbf{r}_4)|)G(234), \quad (6.8)$$

where G denotes a Gaussian correlation wave function for the core nucleus:

$$G(234)=\exp[-b(r_{23}{}^2+r_{34}{}^2+r_{24}{}^2)]. \quad (6.9)$$

Here $b=0.142\ \mu^{-2}$ is fixed to give the spin average, root mean square, nuclear core radius $R_c=1.55$ F given by

$$\bar{R}_c{}^2=(\tfrac{2}{3})\bar{R}_{\rm He^3}{}^2+(\tfrac{1}{3})\bar{R}_{\rm H^3}{}^2-\bar{R}_p{}^2,$$

where $\bar{R}_{\rm He^3}$, $\bar{R}_{\rm H^3}$, and $\bar{R}_p$ are the He^3, H^3,[42] and proton[43] rms charge radii. F in Eq. (6.8) is a variational wave function for the Λ-nucleus correlation:

$$F(r)=\exp(-a_1r^2)+C\exp(-a_2r^2) \quad (6.10)$$

whose parameters have been chosen to obtain the binding energy[44] $B_\Lambda({}_\Lambda\text{He}^4)=2.33$ MeV in the Gaussian potential well of the core nucleus with radius R_w given by

$$R_w{}^2=R_c{}^2+R_v{}^2,$$

where $R_v=0.904$ is the range of a Gaussian potential of the same intrinsic range as a Yukawa potential of range $(2\mu)^{-1}$.[45] The parameters in Eq. (6.10) have the values $a_1=0.214$ F^{-2}, $a_2=0.0384$ F^{-2}, and $C=0.339$.

The Calculation

There are six overlap integrals inside the summation of Eq. (6.6). They correspond to the six transition

[41] Note that the (1/3!) in (6.5) has been canceled by the evaluation of the operator $n(\Lambda')n(p')\bar{n}(\Lambda)\bar{n}(p)$ between two neutron states.

[42] H. Collard, R. Hofstadter, A. Johanssen, R. Parks, M. Ryneveld, A. Walker, M. R. Yearian, R. B. Day, and R. T. Wagner, Phys. Rev. Letters **11**, 132 (1963).

[43] L. N. Hand, D. G. Miller, and R. Wilson, Rev. Mod. Phys. **35**, 335 (1963).

[44] M. Raymund, Nuovo Cimento **32**, 555 (1964).

[45] R. H. Dalitz and B. W. Downs, Phys. Rev. **111**, 967 (1958).

TABLE I. (π^+/π^-) branching ratios calculated in $_\Lambda He^4$. (Experimental ratio: $2.9 \pm 1 \times 10^{-2}$.)

Parameter set	1		2		3		4	
Pseudoscalar F/D ratios	0		$\frac{1}{3}$		(not defined)		$\frac{1}{2}$	
Energy of final π^+ (MeV)	10	(20)	10	(20)	10	(20)	10	(20)
Branching ratios with unitary symmetric phases for decay amplitudes ($\times 100$)								
Charge exchange	0.36	(0.74)	0.36	(0.74)	0.36	(0.74)	0.37	(0.76)
Total (P wave)	0.53	(1.1)	0.47	(1.1)	0.45	(1.0)	0.51	(1.2)
$\Sigma^+ \to n + \pi^+$ (s wave)	0.15	(0.40)	0.46	(0.76)	0.43	(0.70)	0.77	(1.25)
Total (S wave)	0.80	(1.5)	*1.4*	(2.6)	*1.3*	(2.2)	*1.8*	(2.9)
Branching ratios with anti-unitary symmetric phases ($\times 100$)								
Total (P wave)	0.68	(1.5)	0.52	(1.5)	0.60	(1.4)	0.60	(1.4)
Total (S wave)	0.50	(1.0)	0.50	(1.1)	0.40	(0.85)	0.50	(1.0)
Parameters								
Coupling strengths normalized to pion-nucleon vertex $[(f_{\Sigma\Sigma\pi}/f_{NN\pi})^2, (f_{\Sigma\Lambda\pi}/f_{NN\pi})^2]$:	(0.0, 0.941)		(0.154, 0.527)		(0.154, 0.941)		(0.273, 0.417)	
Hard-core radii in fermis (singlet, triplet)	(0.43, 0.54)		(0.39, 0.40)		(0.44, 0.50)		(0.53, 0.51)	

matrix elements to the different terms in an antisymmetrized state of three neutrons in the final wave function. All of the integrations in the overlap integrals may be done analytically because of the convenient properties of the relative Gaussian wave functions except, of course, those in the relative coordinates in which interaction operators occur.

In this way Eq. (6.6) reduces to

$$\Gamma_+ = 2\pi\rho_\pi(q_{\rm av}) \int d\Omega_q \sum_{P'} (-)^{P'} \times \langle \chi | B_2 \int\int d\mathbf{r}_{1'3'} d\mathbf{r}_{13} I_{l'}(\mathbf{r}_{1'3'}, \boldsymbol{\sigma}_1, \boldsymbol{\sigma}_{3'}, \mathbf{q}_{\rm av}) \times \exp[-K r_{1'3'}^2 - 2L(\mathbf{r}_{1'3'} \cdot \mathbf{r}_{13}) - M r_{13}^2] \times \exp[+i\mathbf{q}_{\rm av} \cdot (\mathbf{r}_{l'} - \mathbf{r}_l)] I_l(\mathbf{r}_{13}, \boldsymbol{\sigma}_1, \boldsymbol{\sigma}_3, \mathbf{q}_{\rm av}) | \chi \rangle \quad (6.11)$$

unless the permuted pair $\Lambda' p'$ is the same as the original Λp pair ($\mathbf{r}_{1'3'} = \pm \mathbf{r}_{13}$) in which case the term in Eq. (6.6) reduces further to

$$2\pi\rho_\pi(q_{\rm av}) \int d\Omega_q \langle \chi | B_1 \int d\mathbf{r}_{13} I_{l'}(r_{1'3'}, \boldsymbol{\sigma}_{1'}, \boldsymbol{\sigma}_{3'}, \mathbf{q}_{\rm av}) \times \exp(-S r_{13}^2) \exp(-\mathbf{q}_{\rm av} \cdot (\mathbf{r}_{l'} - \mathbf{r}_l) \times I_l(\mathbf{r}_{13}, \boldsymbol{\sigma}_1, \boldsymbol{\sigma}_3, \mathbf{q}_{\rm av}) | \chi \rangle, \quad (6.12)$$

where B_1, B_2, K, L, M, and S are functions of the wave function parameters which are given in Appendix C, and the complication that there are four terms for each one indicated in (6.11) and (6.12) because of the two-term structure of F in (6.10) is deferred to that place.

Having discussed the structure of the overlap integrals, it is necessary to turn to the evaluation of the spin-dependent factors:

$$\langle \chi(1'2'; 3'4) | I(\mathbf{r}_{1'3'}, \boldsymbol{\sigma}_{1'}, \boldsymbol{\sigma}_{3'}, \mathbf{q}_{\rm av}) \times I(\mathbf{r}_{13}, \boldsymbol{\sigma}_1, \boldsymbol{\sigma}_3, \mathbf{q}_{\rm av}) | \chi(12; 34) \rangle. \quad (6.13)$$

Since transitions occur dominantly from initial relative S states in the Λ–p relative coordinate, the angular momentum properties of the interaction operators may be characterized according to whether they cause transitions to even parity $^1S_0$, $^3S_1$, $^3D_1$, $^3D_2$ states in this coordinate, or odd parity $^1P_1$, $^3P_0$, and $^3P_1$ states associated respectively, with parity conserving and violating interactions in the relative coordinate.

Transitions to orthogonal final states do not give interference terms, with the consequence that the quadratic term in the transition operators in Eq. (6.13) will effectively split into a sum of quadratic terms, each associated with a particular final state. One consequence is that operators from diagrams involving Σ^+ decay will not interfere with those involving Σ^- decay because of their difference in parity expressed in Eq. (4.6). These statements are somewhat complicated when the higher partial waves in the recoil factor $\exp[i\mathbf{q} \cdot (\mathbf{r}_l - \mathbf{r}_{l'})]$ are taken into account. Fortunately, these terms were found unimportant for the $\mathbf{q}_{\rm av}$'s typical of (1.1). In Appendix D the angle and spin-dependent operators not eliminated on general grounds are separated into their spin and space parts and the structure of the final integrals examined.

VII. RESULTS AND CONCLUSIONS

The final integrations in Eqs. (6.11) and (6.12) were performed upon the University of Chicago's IBM-7094 computer.

The results for the charge exchange contributions [Fig. 1(b)] were found to vary by only a few percent for variations of the energy of the exchanged π^0 within the energetically allowed range and the numbers quoted

TABLE II. Observed hypernuclei and their Q values for π^+ decay.

${}_\Lambda Z^A$	Number observed	B_Λ (MeV)[a]	B_p (MeV)[c]	B_{n_1} (MeV)[c]	B_{n_2} (MeV)[c]	Q_+ (MeV)
${}_\Lambda H^3$	76	0.3	2.236	<0	<0	<32.5
${}_\Lambda H^4$	218	2.0[b]	8.48	<0	<0	<24.5
${}_\Lambda He^4$	48	2.3[b]	5.48	6.24	<0	<33.5
${}_\Lambda He^5$	147	3.1	20.8	<0	<0	<11.1
${}_\Lambda He^7$	14	4.0	21.8	<0	<0	<9.2
${}_\Lambda Li^7$	25	5.5	4.653	1.921	<0	<26.8
${}_\Lambda Be^7$	2	4.9	0.6	5.663	7.253	42.4
${}_\Lambda Li^8$	44	6.6	9.985	<0	<0	<18.4
${}_\Lambda Be^8$	4	6.3	5.609	7.253	2.033	32.4
${}_\Lambda Li^9$	10	8.0	12.97	<0	<0	<14.0
${}_\Lambda Be^9$	10	6.5	17.252	2.033	3.7	18.0
${}_\Lambda Be^{10}$	5	9.5	16.885	3.7	<0	<12.3
${}_\Lambda B^{10}$	6	10.6	−0.187	1.665	6.814	33.1
${}_\Lambda B^{11}$	5	10.0	6.587	6.814	−0.503	24.7
${}_\Lambda B^{12}$	8	10.5	11.229	0.504	<0	<13.8
${}_\Lambda C^{13}$	2	10.6	15.956	3.370	4.88	16.7
${}_\Lambda C^{14}$	1	13.2	17.533	4.947	<0	<9.2
${}_\Lambda N^{14}$	1	11.7	1.943	20.18	8.176	49.7

[a] R. Levi Setti, "Hypernuclei" lecture given at the St. Cergue Conference, CERN Geneva, 1963 (unpublished). The figures quoted are for mesonic decays in emulsion. Additional ${}_\Lambda H^3$, ${}_\Lambda H^4$, and ${}_\Lambda He^4$ events have been observed in helium bubble chamber work (Ref. 7).
[b] M. Raymund, Ref. 44.
[c] *Nuclear Data Sheets*, compiled by K. Way *et al.* (Printing and Publishing Office, National Academy of Sciences—National Research Council, Washington 25, D.C., 1962), NRC 61-5.

are with this energy fixed at 20 MeV. The dependence upon final pion energy is stronger: For the 10-MeV average pion energy observed, the (π^+/π^-) branching ratio due to this process alone is about 0.35%. For a 20-MeV final π^+, it is about 0.75%. These numbers vary by only a few percent for variation of the cutoff energy from 120 MeV ($m^2=6$) to 240 MeV ($m^2=12$). It was the smallness of the 0.35% branching ratio compared to the (2.9 ± 1)% experimental branching ratio which led us to consider the other processes of Figs. 1 and 2.

In Table I are displayed the rates calculated for the four listed sets of strong hyperon-pion coupling constants and the four different sets of weak hyperon-pion coupling constants specified in Eqs. (4.6). These rates have been calculated both for 10 and 20 MeV emitted pions although it appears at the moment (see Fig. 4) that an appropriate average energy will be considerably closer to 10 MeV. It can be seen from the table that, as argued, in Sec. I, the contributions of the charge exchange process dominates unless the $\Sigma^+\to n+\pi^+$ decay is S wave, in which case the π^+ emission rate is considerably increased.

The contribution of the Σ^+ virtual state depends very sensitively upon the F/D unitary symmetry-mixing ratio for the baryon-pseudoscalar meson couplings and when $f_{\Sigma\Sigma\pi}$ is held constant in parameter sets 2 and 3 it appears that the sensitivity is, in fact, largely to $f_{\Sigma\Sigma\pi}$. This can be understood through the result obtained in Sec. I, that ${}^1S_0$ initial states are involved most favorably in S-wave Σ^+ decay and the dominant S-wave charge exchange contributions, the triplet states all leading to Pauli forbidden final two-neutron states. The ${}^1S_0$ Σ–N state is sensitive to $f_{\Sigma\Sigma\pi}$ because it is contributed to strongly by two-pion exchange diagrams proportional to $f_{\Sigma\Lambda\pi}f_{\Sigma\Sigma\pi}$ while one-pion exchange terms proportional only to $f_{\Sigma\Lambda\pi}$ lead dominantly to tensor intermediate states.

It can be seen from Table I that, unless the $\Sigma^+\to n+\pi^+$ decay is S-wave, the considerations of this paper do not substantially improve the discrepancy between theory and experiment present[23] in a model assuming only the charge-exchange process of Fig. 1(b). If the decay is S-wave, improvement is greatest when the relative phases of the Λ and Σ decay couplings are chosen according to Gell-Mann's[9] unitary symmetry arguments (indicated as "unitary symmetric phases" in Table I. Opposite choice indicated as "anti-unitary symmetric phases.") Then agreement with experiment appears best for an F/D mixing ratio near $\frac{1}{3}$ not in strong disagreement with the current evidence discussed in Sec. IV.

To summarize then, for currently favored values of the strong coupling constants, our model gives best agreement with experiment if the $\Sigma^+\to n+\pi^+$ decay is S wave, and the Σ and Λ decay amplitudes are chosen to have relative phases given by unitary symmetry. The calculated rate is about 3 times greater than for the alternative parameter choices. Our faith in the result is increased by the fact that the major competing contribution is found to be the well-understood S-wave charge exchange process. If the $\Sigma^+\to n+\pi^+$ decay is P wave, or antiunitary symmetric phases are used, the calculated rate is not very much greater than that due to charge exchange. These results are unaffected by raising the completeness approximation cutoffs to as high an energy as 250 MeV ($m^2=12$), which is good evidence also that our completeness approximation does not result in great overestimates. If our results are interpreted as evidence for S-wave $\Sigma^+\to n+\pi^+$

decay, then it would appear that the R invariance which has been suggested for nonleptonic decay interactions[8,10] with its P-wave prediction may not hold.

VIII. THE π^+ DECAYS OF OTHER HYPERNUCLEI

Eight out of ten observed π^+ hypernuclear decays have been identified as decays of the species ${}_\Lambda He^4$. The question naturally arises: Why?

Part of the answer is that ${}_\Lambda He^4$ is one of the more frequently occurring hypernuclei (see Table II). However, there are additional factors which tend to favor this hypernucleus as a π^+ emitter relative to most other light hypernuclei and relative to all those occurring with comparable abundance.

(i) ${}_\Lambda He^3$, the only known hypernucleus lighter than ${}_\Lambda He^4$, is not tightly enough bound to favor a Λ–p interaction (see Table II).

(ii) For other hypernuclei as heavy as or heavier than ${}_\Lambda He^4$, such as the very common species ${}_\Lambda H^4$ and ${}_\Lambda He^5$ (see Table II), the π^+ emission rate is affected most by the energy release (Q value) of the decay. The unbound levels of the final nuclear systems lie quite high generally relative to those states energetically accessible. In another manner of speaking, this effect is due to the Pauli suppression discussed in Sec. I which does not affect the π^- or π^0 decays of light hypernuclei as strongly, because the final nucleons associated with these decays can go to low-energy states in the region outside the core nucleus. Evidence for the strength of the Pauli suppression effect for the π^+ decay rates is provided in a result of our calculation, that only the "allowed" ${}^1S_0 \to {}^1S_0$ transitions (see Sec. I) for the $\Lambda - p \to n - n$ pair are not substantially reduced below the corresponding "classical rates" (see Sec. VI). Further evidence for the strong favoring of high-energy final states of the nucleon system is provided by the low median energy of the π^+ mesons observed (see Fig. 4).

These effects suggest a simple model for the dependence upon the hypernucleus of the π^+ decay rate: It increases strongly with increased energy release. The Q values of the decays in this model will depend qualitatively upon two features: the binding energy of the Λ and the ratio Z/A for initial hypernucleus ${}_\Lambda Z^A$. In fact, the Q value could be written

$$Q_+ = Q_0 + B_{n_1} + B_{n_2} - B_\Lambda - B_p, \tag{8.1}$$

where

$$Q_0 = M_\Lambda + M_p - 2M_n - M_{\pi^+} = 35 \text{ MeV}. \tag{8.2}$$

B_Λ is the binding energy of Λ, B_p is the binding energy of the most lightly bound proton of the core nucleus and B_{n_1}, B_{n_2}, the energies of the lowest states accessible to the decay neutrons in the final state.

Experimentally, B_Λ increases for the light hypernuclei from about 2.2 MeV for (${}_\Lambda H^4$, ${}_\Lambda He^4$) to 12.5 MeV for (${}_\Lambda C^{14}$, ${}_\Lambda N^{14}$) (see Table II). B_p and B_n vary more according to the shell structure of the core nucleus. In Table II their values are given where they are known. When they are unknown, the associated systems $(Z-1)^{A-2}$, $(Z-1)^{A-1}$, or $(Z-1)^A$ are assumed unbound. If these systems are truly unbound (as most of them assuredly are), the associated values of B_p, B_{n_1}, and B_{n_2} can only be obtained experimentally through a study of resonances in neutron rich systems. In Table II the data known to us are used to give values or upper bounds on the Q_+ for each hypernuclear species.

It can be seen from Table II that, of the common hypernuclei, ${}_\Lambda He^4$ has the most favorable Q value. Other than ${}_\Lambda H^3$, which has been eliminated above for other reasons, its nearest competitor is ${}_\Lambda H^4$ which has one less "stimulating" proton. ${}_\Lambda H^4$ is interesting, although perhaps not significant, in that the event of Blau *et al.*[16] could have this interpretation.[18] Among the rarer hypernuclei, those with the most favorable Q's are ${}_\Lambda N^{14}$, ${}_\Lambda Be^7$, ${}_\Lambda B^{10}$, and ${}_\Lambda Be^8$ in that order. Again it is interesting, although perhaps not significant, that the remaining two π^+-emitting events not interpretable as decays of ${}_\Lambda He^4$, those of Schneps[15] and the Oxford group[17] have interpretations as the decays of ${}_\Lambda Be^7$ or ${}_\Lambda Be^8$.[18]

Thus it appears that this crude model is at least in accord with the meager experimental evidence to date.

ACKNOWLEDGMENTS

I should like to thank R. H. Dalitz who introduced me to several of the techniques used in this calculation and who has been my indispensable critic. I have had several useful discussions on the experimental background with M. Beniston, W. Püschel and M. Raymund of the EFINS emulsion group. B. Lumbert's cheerful advice about the IBM 7090 has made my life much easier. Finally, I would like to thank a number of physicists in Oxford, notably D. Wilkinson, R. Rook, P. S. Fisher, and the members of the emulsion group for many discussions during an earlier version of this calculation; and A. P. Balachandran for reading the manuscript.

APPENDIX A: IDENTIFICATION OF FINAL NUCLEAR STATES

Experimentally, an example of the decays (2.1) in emulsion or bubble chamber is characterized by the track lengths of the two charged particles and the angle between the tracks. The *track length* (or curvature) of the (lightly ionizing) pion gives its energy directly but the energy associated with the charged recoil can only be obtained from its track length by assigning it the mass of a proton, deuteron, or triton. (In the kinetic energy region up to 20 MeV the triton and deuteron kinetic energies are, very roughly, $\frac{3}{2}$ and $\frac{4}{3}$ that of a proton for the same track length.)

The three-body final state (2.1a) may be completely characterized in terms of the energies of two of the final particles and we may put (2.1b) and (2.1c) on the same

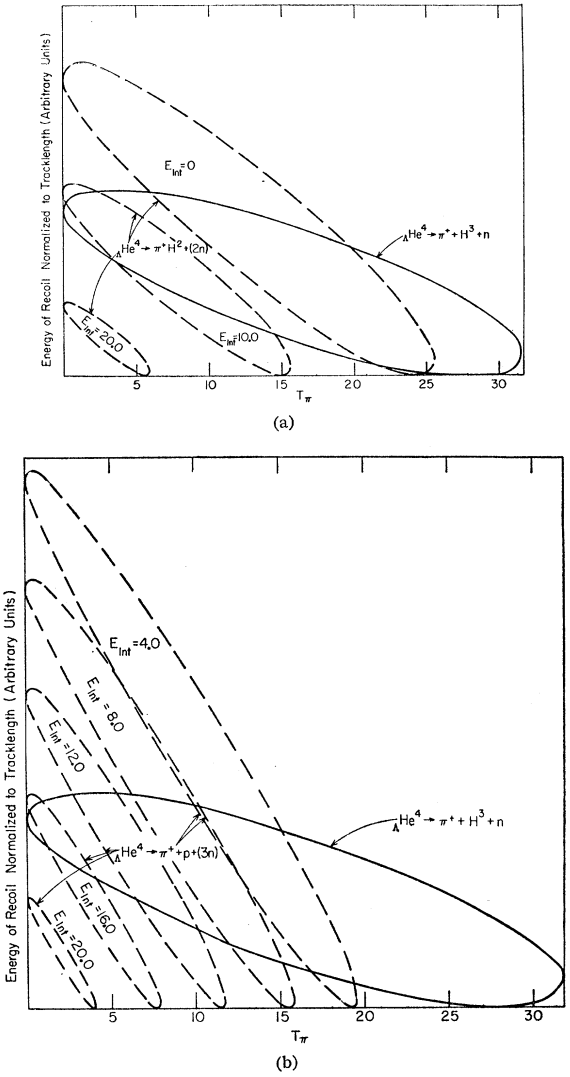

FIG. 6. Dalitz plot of the mode ${}_\Lambda He^4 \to \pi^+ + H^3 + n$ superimposed with plots: (a) for the mode ${}_\Lambda He^4 \to \pi^+ + H^2 + (2n)$ for various internal $(2n)$ energies, (b) for the mode ${}_\Lambda He^4 \to \pi^+ + p + (3n)$ for various internal $(3n)$ energies. The vertical scale is linear in the energies of the charged recoils but is scaled according to their track lengths.

footing by considering their respective two-neutron and three-neutron systems as single bodies with masses depending upon their internal energies. In Figs. 6(a) and 6(b) the three-body phase-space envelopes are plotted for the three final states in terms of the pion and recoil energies. The energies of the recoil particles have been scaled so that, as far as possible, equal heights on the ordinates will represent equal recoil track lengths. It can be seen from these figures that, as far as phase space is concerned, many events can be expected to have track lengths which will not distinguish the final nuclear state. The tendency toward low pion energies discussed in Sec. I does not relieve the situation. Only in cases of very high pion[4] or proton[3] energy can unique assignments be made on the basis of track length to the modes (2.1a) and (2.1c), respectively.

Is it possible to distinguish on the basis of angle then? With sufficient experimental accuracy the answer is yes. It would be possible to distinguish (2.1a) from (2.1b) or (2.1c) with arbitrarily great confidence because a measurement of the track lengths gives a predicted angle for (2.1a) about which the angles of (2.1b) and (2.1c) would be distributed evenly. Unfortunately, the experimental accuracy is not this good. It is best for emulsion, but even there we estimate as the result of some work by Raymund[46] that measurements of (1.2a) would result in errors corresponding to an inaccuracy of the order of 2 MeV in the binding energy.

Raymund has made a calculation of the binding energy of ${}_\Lambda He^5$ using only the data obtainable from the configuration of the π^- and He^4 tracks in 124 examples of the decay mode

$$ {}_\Lambda He^5 \to He^4 + p + \pi^- .$$

The standard deviation on the binding energy is about 1.1 MeV but when only the 6 events with pions of less 17 MeV are analyzed [corresponding more closely to (1.1)] it goes to about 2 MeV. A variation of 2 MeV in the observed energy results in typical variations of about 35° in the calculated angle so that without improved resolution any one event will usually have an ambiguous interpretation and a statistical analysis of a large number of events is necessary before branching ratios for the modes (1.2) are to be obtained.

APPENDIX B: RESULTS CALCULATED IN STATIC APPROXIMATION

The interaction operators associated with the diagrams of Fig. 2 may be written:

Σ^- *decay:*

$$\frac{2\sqrt{2} f(\Sigma_-^-) f_{\Sigma\Lambda\pi} f_{NN\pi}}{(2\omega_q)^{1/2}(2\pi)^{9/2}(M_\Sigma - M_\Lambda)} \times \int d\mathbf{k} \left\{ \left[S(\Sigma_-^-) + P(\Sigma_-^-) \frac{(\boldsymbol{\sigma}_\Lambda \cdot \mathbf{k})}{q_\Sigma} \right] \times [(\boldsymbol{\sigma}_\Lambda \cdot \mathbf{q}_{av})(\boldsymbol{\sigma}_p \cdot \mathbf{k}) \exp(i\mathbf{k}\cdot\mathbf{r})(1/\omega_k^2) \right\} . \quad \text{(B1)}$$

Λ *decay:*

$$\frac{-4 f(\Lambda_0^0) S(\Lambda_0^0)}{(2\omega_q)^{1/2}(2\pi)^{9/2}(M_\Lambda - M_N)} (\boldsymbol{\sigma}_\Lambda \cdot \mathbf{q}_{av}) \times \int d\mathbf{k} [(\boldsymbol{\sigma}_p \cdot \mathbf{k}) \exp(i\mathbf{k}\cdot\mathbf{r})(1/\omega_k^2)], \quad \text{(B2)}$$

[46] Reference 44 and private communication.

where $\omega_k^2 = k^2+1$, $r = r_\Lambda - r_p$; $q_\Lambda = 0.72$ and $q_\Sigma = 1.365$ are the pion momenta from free Λ and free Σ decay, respectively, and the coupling constants have been defined in Sec. IV.

Most of the integrals in (B1)–(B2) diverge for large k. This results in a singularity at $r=0$. For $r>0$ the integrals are finite, as may be ascertained by subtracting terms corresponding to the Fourier transforms of the singularities at $r=0$. Alternatively, the functions for $r>0$ may be obtained by ignoring the divergent character of the integrals and calculating them according to Cauchy's theorem in terms of the singularities of the integrand in the finite plane. This can be done because the integral along the contour at infinity contributes only to the singularities at $r=0$. The integrals in (B1) and (B2) are expressible in terms of spherical Hankel functions[47]:

$$\int d\mathbf{k}(\boldsymbol{\sigma}_p\cdot\mathbf{k})\exp(i\mathbf{k}\cdot\mathbf{r})\left(\frac{1}{\omega_k^2}\right)=2\pi^2(\boldsymbol{\sigma}_p\cdot\hat{r})h_1^{(1)}(ir)\,, \quad \text{(B3)}$$

$$\int d\mathbf{k}(\boldsymbol{\sigma}_\Lambda\cdot\mathbf{k})(\boldsymbol{\sigma}_p\cdot\mathbf{k})\exp(i\mathbf{k}\cdot\mathbf{r})\left(\frac{1}{\omega_k^2}\right)$$
$$=-2\pi^2 T_{\Lambda p}h_2^{(1)}(ir)+2\pi^2(\boldsymbol{\sigma}_\Lambda\cdot\boldsymbol{\sigma}_p/3)h_0^{(1)}\,. \quad \text{(B4)}$$

Cutoffs for large k in (B3)–(B4) canceling the highly singular components of the operators associated with transitions with $\Delta l \geqslant 1$ in the Λ–p coordinate can be most simply introduced by the substitution

$$\frac{1}{\omega_k^2}\to C\left[\frac{1}{\omega_k^2}-\frac{a}{(\Omega_k)^2}-\frac{a'}{(\Omega_k')^2}\right],$$

where

$$(\Omega_k)^2=k^2+m^2;\quad (\Omega_k')^2=k^2+(m')^2;\quad (m')^2=m^2+0.1;$$
$$C=\frac{(m^2+1)[(m')^2+1]}{(m^2-1)[(m')^2-1]};\quad a=\frac{(m')^2-1}{(m')^2-m^2};$$
$$a'=\frac{m^2-1}{m^2-(m')^2}\,.$$

C has been chosen so that the cutoff has no effect at the most important k's near $k=1$. The singular behavior being canceled is associated in completeness approximation primarily with transitions to energetically forbidden final states (large k) as the centrifugal barrier suppresses transitions to lower energy final states. The subtraction terms have the same functional dependence upon mr and $m'r$ as the unsubtracted ones on the right sides of (B3)–(B4) have upon r.

Introduction of a cutoff into the singular P-wave charge exchange interaction operator results in the change:

$$\left(\frac{1}{r}-iq_0\right)\exp(iq_0r)\to\frac{(m^2+1)}{(m^2+q_0^2)}\left[\left(\frac{1}{r}-iq_0\right)\exp(iq_0r)-\left(\frac{1}{r}+m\right)\exp(-mr)\right].$$

A reasonable cutoff mass chosen to leave the integrands unaffected for energetically accessible momentum transfers and suppress them for $k>2$ is $m^2\approx 6$. Fortunately, however, our conclusions in Sec. VII are not strongly affected by variations of the values of the cutoffs up to very large values (see Sec. VII).

APPENDIX C. WAVE FUNCTION OVERLAP INTEGRALS

A convenient starting point for the derivation of the forms (6.11) and (6.12) from (6.6) is the representation of the initial space wave function as a product of S-wave shell-model wave functions relative to the center of mass.[48]

$$\phi(12;34)=(N)^{-1/2}\sum_{i=1,2}C_i\exp[-\alpha_i r_1^2 -\beta(r_2^2+r_3^2+r_4^2)]\delta(\mathbf{r}_1+\mathbf{r}_2+\mathbf{r}_3+\mathbf{r}_4)\,. \quad \text{(C1)}$$

The summation in (C1) is over the two Gaussians in the Λ–He^3 variational wave function (6.10). In terms of the parameters representing the initial wave function in (6.9) and (6.10), $\alpha_i=16a_i/9-b$, $\beta=3b$, $C_1=1$, $C_2=C$. The integrals in (6.6) may then be written explicitly

$$\frac{1}{N}\sum_{i,j=1,2}C_iC_j\int\int\int\int d\mathbf{r}_1 d\mathbf{r}_2 d\mathbf{r}_3 d\mathbf{r}_4 I_{l'} \times\exp[-\alpha_i r_{1'}^2-\alpha_j r_1^2 -\beta(r_{2'}^2+r_2^2+r_{3'}^2+r_3^2+2r_4^2)] \times\exp[-i\mathbf{q}_{\rm av}\cdot(\mathbf{r}_{1'}-\mathbf{r}_1)]I_l\delta(\mathbf{r}_1+\mathbf{r}_2+\mathbf{r}_3+\mathbf{r}_4)\,, \quad \text{(C2)}$$

where 1′, 2′, 3′ are some permutation of 1, 2, 3. If the exponential in the integrand due to the wave function overlap terms is abbreviated as $\exp[-Ar_1^2-Br_2^2-Cr_3^2-Dr_4^2]$ the constants in Eqs. (6.11) and (6.12) can be obtained by straightforward changes of variables and integrations as

$$E=A+B+C+9D\,,$$
$$K=[(A+C)(B+D)-4BD]/E\,,$$
$$L=[D(A-2B-2C)-BC]/E\,,$$
$$M=[(A+B)(C+D)+4CD]/E\,,$$
$$S=K-L^2/M\,,$$
$$N=\sum_{i,j=1,2}C_iC_j(\pi)^{9/2}/[E(KM-L^2)]^{3/2},$$
$$B_2(i,j)=(1/N)C_iC_j(\pi/E)^{3/2},$$
$$B_1(i,j)=(1/N)C_iC_j(\pi^2/ME)^{3/2}.$$

[47] L. I. Schiff, *Quantum Mechanics* (McGraw-Hill Book Company, Inc., New York, 1955), 2nd ed., p. 79.

[48] In order to avoid inessential complications, we have neglected the Λ-nucleon mass difference in transformations of coordinates.

TABLE III. Permutations and associated parameters.

	$(-)^P$	Permutation 1′	2′	3′	r_{13}	$r_{1'3'}$	$E_{ij}K_{ijk}$	$E_{ij}L_{ijk}$	$E_{ij}M_{ijk}$
(1)	+	1	2	3	r_{13}	r_{13}	$4\beta(\alpha_i+\alpha_j+6\beta)$	$2\beta(\alpha_i+\alpha_j-10\beta)$	K_1
(2)	−	3	2	1	r_{13}	r_{13}	$(\alpha_i+3\beta)(\alpha_j+3\beta)+8(\alpha_j+\beta)\beta$	$2\beta(\alpha_i-3\alpha_j-6\beta)$	K_1
(3)	+	2	3	1	r_{13}	r_{12}	K_2	L_2	K_2
(4)	+	3	1	2	r_{13}	r_{23}	$K_2{}^T$	$2\beta(\alpha_j-3\alpha_i-6\beta)$	K_1
(5)	−	1	3	2	r_{13}	r_{12}	K_1	L_1	K_1
(6)	−	2	1	3	r_{13}	r_{23}	$(\alpha_i+3\beta)(\alpha_j+3\beta)+8(\alpha_i+\beta)\beta$	$-\alpha_i\alpha_j-5(\alpha_i+\alpha_j)\beta-5\beta^2$	K_2
		$E_{ij}=\alpha_i+\alpha_j+22\beta$							

In Table III, K, L, M, and E are tabulated for each permutation and set of α_i, α_j, β.

APPENDIX D: SPIN MATRIX ELEMENTS AND ANGULAR INTEGRATION

A complete list of the spin-dependent operators which occur in our interaction operators is as follows:

(a) $T=(\boldsymbol{\sigma}_1\cdot\hat{r})(\boldsymbol{\sigma}_3\cdot\hat{r})-\frac{1}{3}(\boldsymbol{\sigma}_1\cdot\boldsymbol{\sigma}_3)$;

(b) $(\boldsymbol{\sigma}_1\cdot\mathbf{q}_{\rm av})T/q_\Sigma$;

(c) $T(\boldsymbol{\sigma}_1\cdot\mathbf{q}_{\rm av})$;

(d) $i(\boldsymbol{\sigma}_1\cdot\mathbf{q}_{\rm av})(\boldsymbol{\sigma}_3\cdot\hat{r})$;

(e) $2i(\mathbf{q}_{\rm av}\cdot\hat{r})+[\boldsymbol{\sigma}_3\cdot(\mathbf{q}_{\rm av}\times\hat{r})]$;

(f) $P_s=\frac{1}{4}[1-(\boldsymbol{\sigma}_\perp\cdot\boldsymbol{\sigma}_3)]$;

(g) $P_T=\frac{1}{4}[3+(\boldsymbol{\sigma}_1\cdot\boldsymbol{\sigma}_3)]$;

(h) $(\boldsymbol{\sigma}_1\cdot\mathbf{q}_{\rm av})P_S/q_\Sigma$;

(i) $(\boldsymbol{\sigma}_1\cdot\mathbf{q}_{\rm av})P_T/q_\Sigma$;

(j) $(\boldsymbol{\sigma}_1\cdot\boldsymbol{\sigma}_3)(\boldsymbol{\sigma}_1\cdot\mathbf{q}_{\rm av})/3q_\Sigma$;

(k) 1.

If we give a matrix whose entries are zero or one, depending upon whether the product of the two operators corresponding to a row and column have a zero or nonzero matrix element when partial waves of the recoil factor in the coordinates r_{13} and $r_{1'3'}$ of the (short-ranged) interaction operators are ignored ("low recoil approximation"), the only off-diagonal nonzero entries taking into account all selection rules will be for the combinations (d)(e), (f)(g), (h)(i), (g)(k). The matrix elements of those nonvanishing product operators independent of the directions $\hat{r}_{13}$ and $\hat{r}_{1'3'}$ may be evaluated immediately upon integration over $\Omega_{\bar{q}}$. In Table IV a number of convenient spin operator matrix elements

$$\langle\chi(1'2';3'4')\,|\,O(\sigma_{1'},\sigma_{3'},\sigma_1,\sigma_3)\,|\,\chi(1,2;3,4)\rangle$$

associated with these products are tabulated.

The coordinate-dependent products are either linear or quadratic in both $\hat{r}_{13}$ and $\hat{r}_{1'3'}$ and contain no terms proportional to $(r_{13})^2$ or $(r_{1'3'})^2$. This reduces the possible forms to two:

$$\sum_{m'm} Y_1{}^{m'}(\theta',\varphi')Z_{m'm}{}^P(\boldsymbol{\sigma}_{1'},\boldsymbol{\sigma}_{3'},\boldsymbol{\sigma}_1,\boldsymbol{\sigma}_3)Y_1{}^m(\theta,\varphi)\,, \quad \text{(D1a)}$$

$$\sum_{m'm} Y_2{}^{m'}(\theta',\varphi')Z_{m'm}{}^D(\boldsymbol{\sigma}_{1'},\boldsymbol{\sigma}_{3'},\boldsymbol{\sigma}_1,\boldsymbol{\sigma}_3)Y_2{}^m(\theta,\varphi)\,, \quad \text{(D1b)}$$

where Z^P and Z^D are functions of the spin operators with, in general, quite complicated transformation properties. Fortunately, however, our concern is only with those Z's which transform as scalars[49] since, in Eq. (6.6), their expectation value with respect to a spin-zero state is taken, Eqs. (D1) then become:

$$\tfrac{4}{3}\pi\sum_m(-)^m Y_1{}^m(\theta',\varphi')Y_1{}^{-m}(\theta,\varphi)Z^P(\boldsymbol{\sigma}_{1'},\boldsymbol{\sigma}_{3'},\boldsymbol{\sigma}_1,\boldsymbol{\sigma}_3)\,, \quad \text{(D2a)}$$

$$\tfrac{4}{5}\pi\sum_m(-)^m Y_2{}^m(\theta',\varphi')Y_2{}^{-m}(\theta,\varphi)Z^D(\boldsymbol{\sigma}_{1'},\boldsymbol{\sigma}_{3'},\boldsymbol{\sigma}_1,\boldsymbol{\sigma}_3)\,, \quad \text{(D2b)}$$

where Z^P, Z^D may most easily be obtained from the

TABLE IV. Useful spin matrix elements.

Permutations: 1′2′3′ =	123	321	231	312	132	213
$P_S(1'3')P_S(13)$	1/4	−1/4	−1/8	−1/8	1/8	1/8
$P_S(1'3')P_T(13)$	0	0	−3/8	3/8	3/8	−3/8
$P_T(1'3')P_S(13)$	0	0	3/8	−3/8	3/8	−3/8
$P_T(1'3')P_T(1'3')$	3/4	3/4	−3/8	−3/8	−3/8	−3/8
$P_S(1'3')(\boldsymbol{\sigma}_{1'}\cdot\boldsymbol{\sigma}_1)P_S(13)$	3/4	3/4	3/8	3/8	3/8	3/8
$P_S(1'3')(\boldsymbol{\sigma}_{1'}\cdot\boldsymbol{\sigma}_1)P_T(13)$	0	0	9/8	3/8	9/8	3/8
$P_T(1'3')(\boldsymbol{\sigma}_{1'}\cdot\boldsymbol{\sigma}_1)P_S(13)$	0	0	3/8	9/8	9/8	3/8
$P_T(1'3')(\boldsymbol{\sigma}_{1'}\cdot\boldsymbol{\sigma}_1)P_T(13)$	9/4	3/4	−3/8	−3/8	−9/8	15/8

[49] Remember that in the low-recoil approximation the angular dependence of the recoil factor is dropped.

TABLE V. Spin operators derived from coordinate-dependent operators.

Operator	Z^l
$l=D$	
(a) $T'T$	$(1/15)[(\boldsymbol{\sigma}_{1'}\cdot(\boldsymbol{\sigma}_{3'}\cdot\boldsymbol{\sigma}_3)\boldsymbol{\sigma}_1)+(\boldsymbol{\sigma}_{3'}\cdot(\boldsymbol{\sigma}_{1'}\cdot\boldsymbol{\sigma}_3)\boldsymbol{\sigma}_1)-\frac{2}{3}(\boldsymbol{\sigma}_{1'}\cdot\boldsymbol{\sigma}_{3'})(\boldsymbol{\sigma}_1\cdot\boldsymbol{\sigma}_3)]$
(b) $T'(\boldsymbol{\sigma}_{1'}\cdot\boldsymbol{\sigma}_1)T$	$(1/15)[(\boldsymbol{\sigma}_{1'}\cdot(\boldsymbol{\sigma}_{3'}\cdot\boldsymbol{\sigma}_3)\boldsymbol{\sigma}_1)+(\boldsymbol{\sigma}_{3'}\cdot(\boldsymbol{\sigma}_{1'}\cdot\boldsymbol{\sigma}_3)\boldsymbol{\sigma}_1)-\frac{2}{3}(\boldsymbol{\sigma}_{1'}\cdot\boldsymbol{\sigma}_{3'})(\boldsymbol{\sigma}_1\cdot\boldsymbol{\sigma}_3)][1+2\delta_{11'}]$
(c) $(\boldsymbol{\sigma}_{1'}\cdot T'T\boldsymbol{\sigma})$	$(1/15)(\boldsymbol{\sigma}_{1'}\cdot[(\boldsymbol{\sigma}_{1'}\cdot(\boldsymbol{\sigma}_{3'}\cdot\boldsymbol{\sigma}_3)\boldsymbol{\sigma}_1)+(\boldsymbol{\sigma}_{3'}\cdot(\boldsymbol{\sigma}_{1'}\cdot\boldsymbol{\sigma}_3)\boldsymbol{\sigma}_1)-\frac{2}{3}(\boldsymbol{\sigma}_{1'}\cdot\boldsymbol{\sigma}_{3'})(\boldsymbol{\sigma}_1\cdot\boldsymbol{\sigma}_3)]\boldsymbol{\sigma}_1)$
$l=P$	
(d) $(\boldsymbol{\sigma}_{3'}\cdot\hat{r}')(\boldsymbol{\sigma}_{1'}\cdot\boldsymbol{\sigma}_1)(\boldsymbol{\sigma}_3\cdot\hat{r})$	$\frac{1}{3}(\boldsymbol{\sigma}_{3'}\cdot(\boldsymbol{\sigma}_{1'}\cdot\boldsymbol{\sigma}_1)\boldsymbol{\sigma}_3)$
(e) $(\boldsymbol{\sigma}_1\cdot\hat{r}')(\boldsymbol{\sigma}_3\cdot\hat{r})$	$\frac{1}{3}(\boldsymbol{\sigma}_1\cdot\boldsymbol{\sigma}_3)$
(f) $(\boldsymbol{\sigma}_{1'}\cdot\hat{r})(\boldsymbol{\sigma}_{3'}\cdot\hat{r}')$	$\frac{1}{3}(\boldsymbol{\sigma}_{1'}\cdot\boldsymbol{\sigma}_{3'})$
(g) $(\boldsymbol{\sigma}_{3'}\cdot\hat{r}')(\boldsymbol{\sigma}_3\cdot\hat{r})$	$\frac{1}{3}(\boldsymbol{\sigma}_{3'}\cdot\boldsymbol{\sigma}_3)$

Spin matrix elements

Permutations: $1'2'3' =$	123	321	231	312	132	213
(a)	$\frac{2}{3}$	$\frac{2}{3}$	$\frac{2}{3}$	$\frac{2}{3}$	$\frac{2}{3}$	$\frac{2}{3}$
(b)	2	$\frac{2}{3}$	$\frac{2}{3}$	$\frac{2}{3}$	2	$\frac{2}{3}$
(c)	2	2	$\frac{2}{3}$	$\frac{2}{3}$	$\frac{2}{3}$	$\frac{2}{3}$
(d)	3	$\frac{3}{2}$	$\frac{3}{2}$	$\frac{3}{2}$	$\frac{3}{2}$	3
(e)	0	$\frac{3}{2}$	$\frac{3}{2}$	$-\frac{3}{2}$	$-\frac{3}{2}$	0
(f)	0	$-\frac{3}{2}$	$-\frac{3}{2}$	$\frac{3}{2}$	$-\frac{3}{2}$	0
(g)	3	$\frac{3}{2}$	$-\frac{3}{2}$	$-\frac{3}{2}$	$\frac{3}{2}$	-3

product operators by setting $\theta'=\theta$, $\varphi'=\varphi$ and integrating over all θ, φ. The Z's for the operators encountered in our calculation are given in Table V along with their spin matrix elements.

It only remains to show how convenient the separation of angular and spin dependence in (E2) is for the evaluation of the integrals in Eqs. (6.11) and (6.12). For (6.12) $\theta'=\theta$, $\varphi'=\varphi$, the sums in (D2) simply give one, and the angular integral results in a factor 4π. For (6.11) the situation is slightly more complicated as the wave function overlap factor has an angular dependence, $\exp[-2L(r_{1'3'},r_{13})]$. This factor may be expanded as[50]

$$\exp[-2L(r_{1'3'},r_{13})]=4\pi\sum_{l=0}^{\infty}\sum_{m=-l}^{l}(-)^m j_l(i2Lr_{1'3'}r_{13})\times Y_l^m(\theta',\varphi')Y_l^{-m}(\theta,\varphi). \quad \text{(D3)}$$

After multiplication by (D2a) or (D2b) and integration over the angles of $\hat{r}_{1'3'}$, $\hat{r}_{13}$ we therefore obtain

$$(4\pi)^2 i^l j_l(2lLr_{1'3'}r_{13})Z^l,$$

where $l=P$ and D for (D2a) and (D2b), respectively.

[50] A. R. Edmonds, *Angular Momentum in Quantum Mechanics* (Princeton University Press, Princeton, New Jersey, 1957), pp. 81, 21.